Geological Magazine

www.cambridge.org/geo

Original Article

Cite this article: Sakyi PA, Su B-X, Manu J, Kwayisi D, Anani CY, Alemayehu M, Malaviarachchi SPK, Nude PM, and Su B-C. Origin and tectonic significance of the metavolcanic rocks and mafic enclaves from the Palaeoproterozoic Birimian Terrane, SE West African Craton, Ghana. *Geological Magazine* https://doi.org/10.1017/S001675681900150X

Received: 17 May 2019
Revised: 3 December 2019
Accepted: 10 December 2019

Keywords:
West African Craton; Birimian Terrane; Lawra Belt; Sr–Nd isotopes; subduction; arc setting

Author for correspondence:
Patrick Asamoah Sakyi,
Email: pasakyi@ug.edu.gh

Origin and tectonic significance of the metavolcanic rocks and mafic enclaves from the Palaeoproterozoic Birimian Terrane, SE West African Craton, Ghana

Patrick Asamoah Sakyi[1,2], Ben-Xun Su[2], Johnson Manu[1], Daniel Kwayisi[1,3], Chris Y. Anani[1], Melesse Alemayehu[4,5], Sanjeewa P.K. Malaviarachchi[6], Prosper M. Nude[1] and Ben-Can Su[7]

[1]Department of Earth Science, School of Physical and Mathematical Sciences, University of Ghana, PO Box LG 58, Legon-Accra, Ghana; [2]Key Laboratory of Mineral Resources, Institute of Geology and Geophysics, Chinese Academy of Sciences, PO Box 9825, Beijing 100029, China; [3]Department of Geology, University of Johannesburg, Johannesburg, South Africa; [4]School of Applied Natural Science, Department of Applied Geology, Adama Science and Technology University, PO Box 1888, Adama, Ethiopia; [5]State Key Laboratory of Isotope Geochemistry, Guangzhou Institute of Geochemistry, Chinese Academy of Sciences, Guangzhou 510640, China; [6]Department of Geology, Faculty of Science, University of Peradeniya, Peradeniya 20400, Sri Lanka and [7]PetroChina Co Ltd of Changqing Oilfield Company Eighth Oil Production Plant, Xi'an 710000, China

Abstract

The Palaeoproterozoic Birimian Supergroup of the West African Craton (WAC) consists of volcanic belts composed predominantly of basaltic and andesitic rocks and intervening sedimentary basins composed predominantly of wackes and argillites. Mafic metavolcanic rocks and granitoid-hosted enclaves from the Palaeoproterozoic Lawra Belt of Ghana were analysed for geochemical and Sr–Nd isotopic data to constrain the geological evolution of the southeastern part of the WAC. The metavolcanic rocks display mainly tholeiitic signatures, whereas the enclaves show calc-alkaline signatures. The high SiO_2 contents (48.6–68.9 wt%) of the enclaves are suggestive of their evolved character. The high Th/Yb values of the samples relative to that of the mantle array may indicate derivation of their respective magmas from subduction-modified source(s). The rocks show positive ε_{Nd} values of +0.79 to +2.86 (metavolcanic rocks) and +0.79 to +1.82 (enclaves). These signatures and their Nd model ages (T_{DM2}) of 2.31–2.47 Ga (metavolcanic rocks) and 2.39–2.47 Ga (enclaves) suggest they were probably derived from juvenile mantle-derived protoliths, with possible input of subducted pre-Birimian (Archean?) rocks in their source(s). Their positive Ba–Th and negative Nb–Ta, Zr–Hf and Ti anomalies may indicate their formation through subduction-related magmatism consistent with an arc setting. We propose that the metavolcanic rocks and enclaves from the Lawra Belt formed in a similar island-arc setting. We infer that the granitoids developed through variable degrees of mixing/mingling between basic magma and granitic melt during subduction, when blobs of basic to intermediate parental magma became trapped in the granitic magma to form the enclaves.

1. Introduction

The Palaeoproterozoic Birimian Terrane of the West African Craton (WAC) continues to engage the attention of geoscientists, and has witnessed a surge in research activities to unravel the geological history of the terrane and its broader implications on the WAC. The present-day Earth has reached near-equilibrium between the amount of crust being generated and that being returned to the mantle at subduction zones. Since the Neoarchean Era, there has been no net loss of crustal material of the continental crust. A myriad of evidence supports secular change in crustal processes through time, including magma compositions, mantle temperatures and metamorphic gradients (Spencer *et al.* 2017). A study conducted by Ganne *et al.* (2012) in the Fada N'Gourma region of the WAC in Burkina Faso concluded that modern-style plate tectonics existed during Palaeoproterozoic time. The Paleoproterozoic Era (2.5–1.6 Ga) represents the main episode of crustal growth recorded on present-day continents (Giustina *et al.* 2009) and was characterized by widespread mafic magmatism across previously stabilized Archean crustal domains (e.g. Heaman, 1997; Isley & Abbott, 1999). This global event was related to the assembly of the supercontinent Columbia during Palaeoproterozoic time (e.g. Rogers & Santosh 2002, 2009; Zhao *et al.* 2002, 2004; Meert, 2012). It is therefore suggested that the early orogenic systems formed through subduction–accretionary processes during the Eburnean Orogeny partly created the supercontinent Columbia.

CAMBRIDGE UNIVERSITY PRESS

The Palaeoproterozoic Birimian Terrane of Ghana occupies the southeastern portion of the WAC, and this area has been subject to much research (e.g. Abouchami *et al.* 1990; Eisenlohr & Hirdes, 1992; Taylor *et al.* 1992; Davis *et al.* 1994; Anum *et al.* 2015; Block *et al.* 2015), all aimed at contributing to the better understanding of the geodynamic evolution of the WAC. However, the geochronology, petrogenesis, provenance and tectonic setting of the Palaeoproterozoic Birimian rocks remain the focus of continuous discussion. The tectonic settings proposed by some of the studies so far range from the generation of the Birimian juvenile crust in arc environments (e.g. Sylvester & Attoh, 1992; Asiedu *et al.* 2004; Dampare *et al.* 2005; Sakyi *et al.* 2014, 2018*a*, *b*) to plume-related magmatism (e.g. Abouchami *et al.* 1990; Lompo, 2009). Further, two major models have been proposed to explain the tectonic processes involved in the formation of the Birimian rocks. These are accretionary orogeny (e.g. Abouchami *et al.* 1990; Davis *et al.* 1994; Feybesse & Milési, 1994; Hirdes *et al.* 1996; Hirdes & Davis, 2002) and transcurrent tectonics models (e.g. Doumbia *et al.* 1998).

In the past, geological studies on the Birimian Terrane of Ghana have focused on either the metavolcanic rocks (e.g. Dampare *et al.* 2008, 2009; Senyah *et al.* 2016), metasedimentary rocks (e.g. Asiedu *et al.* 2017) or the granitoids (e.g. Losiak *et al.* 2013; Anum *et al.* 2015; Petersson *et al.* 2016) mostly in southern Ghana.

The northwestern part of Ghana has recently witnessed a couple of studies, all aimed at understanding the geological evolution of the Palaeoproterozoic Birimian Terrane (e.g. de Kock *et al.* 2011; Amponsah *et al.* 2015, 2016*b*; Block *et al.* 2015, 2016*a*, *b*). With the advent of new and improved analytical techniques, most of the studies on the Birimian Terrane in Ghana in the past decade were often limited to individual belts and basins or adjacent belts and basins (e.g. Dampare *et al.* 2008, 2009; Anum *et al.* 2015; Abitty *et al.* 2016; Senyah *et al.* 2016). The aim is to improve on previous works in terms of sample density, and also take advantage of improved analytical techniques to deepen our understanding of the evolution of the Palaeoproterozoic Birimian rocks of the WAC. These studies include a comprehensive zircon U–Pb dating of the granitoids in the Lawra Belt by Sakyi *et al.* (2014) that produced the oldest-published ages of 2211 Ma and 2213 Ma. The study suggested that the emplacement of Birimian granitoids in Ghana may have commenced much earlier than previously reported in the literature. Block *et al.* (2015) carried out petrological and geochronological studies of high-grade ortho- and paragneisses of the eastern Baoulé-Mossi domain, covering an extensive area in northern Ghana, and revealed the exhumation of the lower crust along reverse, normal and transcurrent shear zones and juxtaposed against shallow crustal slices during the Eburnean Orogeny. The study of granitoids in the middle to northern parts of Ghana, notably the Bole-Bulenga and Abulembire domains, revealed that the former is commonly migmatitic whereas the latter is principally made of paragneisses, sometimes migmatitic, intruded by granitoid gneisses emplaced during *c.* 2200–2125 Ma (Agyei Duodu *et al.* 2009; de Kock *et al.* 2009). Block *et al.* (2016*a*) showed that all the different rock types that make up the Palaeoproterozoic crust of northern Ghana were formed together over a prolonged period of *c.* 100 Ma during *c.* 2.21–2.11 Ga, where the tonalite–trondhjemite–granodiorites (TTGs) were derived from the reworking of low-K hydrous mafic crust. The more-felsic rock types were formed by reworking of older felsic crustal rocks. It was further revealed that most of the Palaeoproterozoic Birimian rocks in the Bole–Nangodi Belt do not show any significant variation in geochemical characteristics, suggesting that they may be products of a similar source with varying degrees of evolution and generated in similar tectonic settings (e.g. Block *et al.* 2016*a*).

U–Pb and Hf-isotope studies of detrital zircons from the Palaeoproterozoic Baoulé–Mossi domain (Parra-Avila *et al.* 2016) indicate that, although the zircons generally confirm its juvenile origin, they also indicate reworking of an older crust at a much larger scale than previously recognized. The identification of Archean zircons in the region therefore argues for greater interaction between the Baoulé–Mossi domain and the Archean Kénéma–Man domain. Additionally, zircon U–Pb dating and Hf and O-isotope studies of igneous rocks from the Palaeoproterozoic Baoulé-Mossi domain of the WAC, covering Burkina Faso, Ghana, Guinea and Mali, revealed the juvenile isotopic character of the domain, and further showed that the southern part of the WAC evolved by accretionary processes (Parra-Avila *et al.* 2017, 2018). Similar to the above, zircon U–Pb age and Lu–Hf isotopic data from granites of southern, southeastern and northwestern Ghana suggest juvenile crustal addition with a short period of reworking of Archaean crust within the Palaeoproterozoic Birimian Terrane of Ghana, and provides evidence of subduction-related crustal growth (Petersson *et al.* 2016, 2018). Grenholm *et al.* (2019) also showed that the Birimian Orogen in the southern WAC forms part of a large accretionary–collisional orogenic system that extends into the Reguibat shields in northern WAC and southwards into equivalent crust in the Amazon Craton. They indicated that early evolution of the orogen was characterized by deposition of volcanic–volcanosedimentary successions and emplacement of limited intrusives, with a significant contribution from juvenile sources. It was further concluded that the alternation between compression and extension within the context of regional convergence was a key factor in driving the evolution of the Birimian Orogen and establishing the architecture of the crust exposed in the southern WAC. The presence of enclaves of different compositions, most of which are mafic, is characteristic of the Palaeoproterozoic granitoid intrusions of the Birimian in Ghana. Enclaves within igneous rocks can potentially provide information on the origin and/or evolution of the magma in which they are found. However, they have received little or no attention in the various studies so far carried out in the Birimian terrane of the WAC.

In this paper, we present whole-rock geochemistry and Rb–Sr and Sm–Nd isotopic systematics of mafic to intermediate metavolcanic rocks and granitoid-hosted mafic enclaves from the Lawra Volcanic Belt of the Palaeoproterozoic Terrane of the WAC in Ghana. The study aims to provide further insights and a deeper understanding of the origin, petrogenesis and tectonic emplacement of the volcanic rocks and the enclaves, with the ultimate goal of contributing towards a better understanding of the geodynamic evolution of the WAC.

2. Geological setting

The Palaeoproterozoic Birimian Terrane of Ghana occupies the southeastern part of the WAC (Fig. 1a). The Lawra Volcanic Belt is located in northwestern Ghana (Fig. 1a, b) and represents one out of the six Birimian Volcanic belts in Ghana; the remaining five are the Kibi–Winneba, Ashanti, Sefwi, Bui and Bole–Nangodi belts (e.g. Leube *et al.* 1990). These volcanic belts are separated by intervening NE-trending sedimentary basins, namely the Cape Coast, Kumasi, Sunyani and Maluwe basins (Kesse, 1985). A conspicuous feature of the Birimian terrane of Ghana is the NE–SW

https://doi.org/10.1017/S001675681900150X

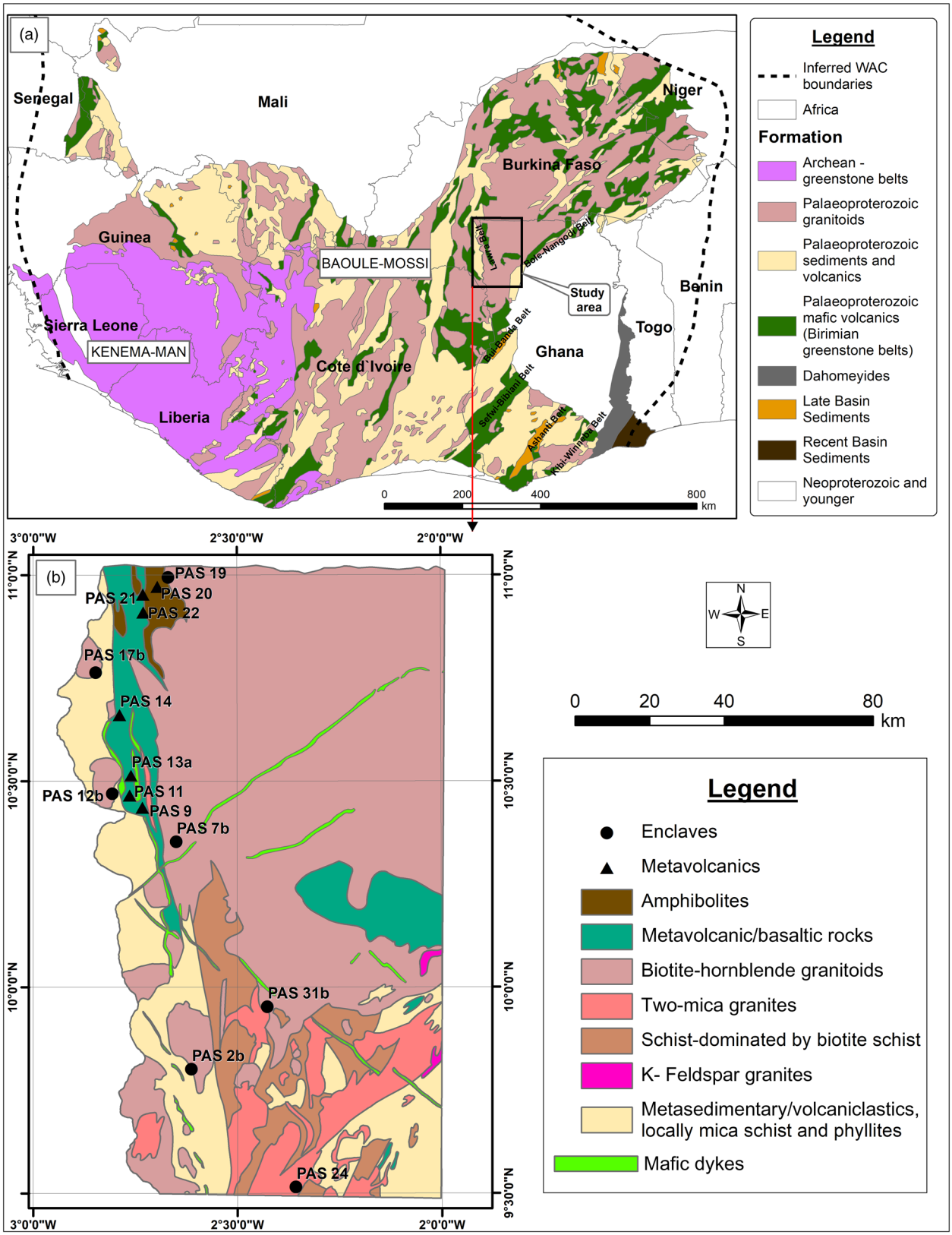

Fig. 1. (Colour online) (a) Geological sketch map of the Man Shield showing the WAC and Palaeoproterozoic Birimian rocks. The location of the study area in northwestern Ghana and the various volcanic belts are also shown. (b) Geological sketch map of the Lawra Volcanic Belt, showing the distribution of the various rock units. Sample positions are also indicated. Modified after Agyei Duodu *et al.* (2009).

trend of all the volcanic belts except for the Lawra Belt, which trends nearly N–S (Leube *et al.* 1990; Hirdes *et al.* 1992). The Lawra Belt marks the southern side of the Proterozoic Boromo greenstone belt that extends through southern and central Burkina Faso (Béziat *et al.* 2000; Baratoux *et al.* 2011). On the other hand, the basins contain metasedimentary rocks comprising dacitic volcaniclastics, wackes and argillites, as well as granitoids, occurring in varying proportions (Leube *et al.* 1990).

The Lawra Volcanic Belt (Fig. 1b) is made up of metamorphosed volcanic rocks comprising mainly tholeiitic subalkaline meta-basalts, meta-andesites, porphyritic calc-alkaline hornblende-actinolite-schists and amphibolites (e.g. Jessell *et al.* 2012; Amponsah *et al.* 2016*a*). The metasedimentary rocks in the belts are detrital volcanogenic sediments, comprising mainly volcaniclastics, volcaniclastic wackes, argillites and tuffs that have been metamorphosed to schists, phyllites and greywackes (e.g. Leube *et al.* 1990). Occurring in the transition zones between the volcanic belts and sedimentary basins are different types of chemical sediments (e.g. cherts, gondites and sulphide- and carbonate-bearing rocks), pyroclastic-volcaniclastic and volcanic rocks (e.g. Leube *et al.* 1990). The volcano-sedimentary terranes are intruded by granitoids of various ages, but two main suites are recognized; the Dixcove-type granitoids intrude the Birimian volcanic rocks and are interpreted to be coeval with them (Eisenlohr & Hirdes, 1992). They are metaluminous and comprise hornblende- to biotite-bearing granodiorites to diorites, monzonites and syenites. In contrast, the Cape Coast-type granitoids intrude the Birimian sedimentary rocks and are mainly peraluminous, two-mica granodiorites, with lesser hornblende- and biotite-bearing granodiorites (Eisenlohr & Hirdes, 1992). These granitoids are interpreted to have been emplaced synchronously with the major deformation event that affected the rocks of the Birimian Supergroup (Eisenlohr & Hirdes, 1992).

3. Materials and methods

Samples for this study are seven mafic to intermediate metavolcanic rocks and seven granitoid-hosted enclaves from the Lawra Belt. Because of the weathered nature of the metavolcanic rocks, and the fact that sampling was restricted to the surface, our sampling protocol focused mainly on road-cuts where fresh samples were exposed; this is the main reason for the limited number of metavolcanic samples used for the study.

3.a. Major and trace elements

Major- and trace-element abundances in the 14 samples were measured at the Institute of Geology and Geophysics, Chinese Academy of Sciences (IGGCAS) in Beijing. Chips of whole-rock samples free from any weathered surface were crushed and ground in an agate mill to c. 200 mesh (74 μm). For major-element analysis, approximately 0.5 g of the rock powder was mixed with 5 g of $Li_2B_4O_7$ and three drops of NH_4Br, and the mixture was fused in a furnace to form a glass disk. Major elements were determined on fused glass beads using Shimadzu X-ray fluorescence (XRF-1500), operating with a current of 50 mA and voltage of 50 kV. A detailed description of the analytical procedures is reported in Chu *et al.* (2009).

Trace elements were determined by inductively coupled plasma – mass spectrometry (ICP-MS) using an Agilent 7500a system. The analyses were carried out following the procedures described in Chu *et al.* (2009). Analytical precisions were generally better than 5%, while analytical uncertainties were 1–3% for elements present in concentrations of >1 wt% and about 10% for elements present in concentrations of <1 wt%.

3.b. Rb–Sr and Sm–Nd isotopes

Six metavolcanic and three enclave samples were analysed for Rb–Sr and Sm–Nd isotopes using a VG-354 thermal ionization magnetic sector mass spectrometer at the State Key Laboratory of Lithospheric Evolution, Institute of Geology and Geophysics, Chinese Academy of Sciences in Beijing. The procedures followed for chemical separation and isotopic analyses are described in Zhang *et al.* (2001). Procedural blanks were <100 pg for Rb, 200 pg for Sr, <20 pg for Sm and <50 pg for Nd. Measured $^{87}Sr/^{86}Sr$ and $^{143}Nd/^{144}Nd$ ratios were corrected for mass-fractionation using $^{86}Sr/^{88}Sr = 0.1194$ and $^{146}Nd/^{144}Nd = 0.7219$, respectively. During the period of data collection, the measured values for the NBS987-Sr and JNdi-Nd standards were $^{87}Sr/^{86}Sr = 0.710245 \pm 20$ ($n = 10$) and $^{143}Nd/^{144}Nd = 0.512125 \pm 15$ ($n = 8$). Uncertainties for Rb/Sr and Sm/Nd ratios were <2% and <0.5%, respectively.

4. Results

4.a. Field observations and petrography

Metavolcanic rocks in the Lawra Belt occur in restricted locations, and commonly occur as disconnected outcrops or isolated hills; in some cases, they display extensive exposure. For example, in the vicinity of the Yagha community, located about 18 km NW of Nadowli, the exposed meta-basalts are up to *c.* 850 m long but have experienced extensive surface weathering. In other locations, the disconnected outcrops are sub-rounded at the base with dimensions ranging from *c.* 80 m by 60 m to *c.* 100 m by 80 m. A few relatively small outcrops measuring up to 50 m in diameter at the base also occur in the area. The granitoid intrusions occur in close proximity to the metavolcanic rocks. They are generally less deformed compared with the metavolcanic rocks and contain oriented enclaves with mafic to intermediate compositions. In some areas, the orientation of the enclaves is subparallel to the metamorphosed volcanic rocks. However, a few sizeable rocks are less ellipsoidal and are characterized by curved boundaries. Because of the altered nature of the metavolcanic rocks, sampling on the surface was avoided. Instead, we relied on exposures in road-cuts, notably newly constructed feeder roads where relatively fresh surfaces were exposed. Although the field relations indicate that the metavolcanic rocks are intruded by belt-type granitoids, individual suites of metavolcanic rocks are generally devoid of cross-cutting igneous bodies. Rather, the granitoid intrusions are characterized by criss-crossing quartz veins and dykes of other igneous rocks.

4.a.1. Metavolcanic rocks

The metavolcanic rocks consist of mainly metamorphosed basalts and basaltic andesites, with minor andesites and amphibolites. The metavolcanic rocks have generally experienced greenschist facies metamorphism (Abouchami *et al.* 1990; Amponsah *et al.* 2016*a*) and various degrees of alteration; these have subsequently overprinted the primary minerals with preserved pseudomorphs (Fig. 2a), evident from the presence of secondary minerals such as actinolite, epidote, sericite and chlorite. The metabasalts (Fig. 2a–c) are fine-grained and dark green to dark grey. They are massive or weakly foliated, aphyric and sparsely porphyritic, with less than 10% phenocrysts set in a microcrystalline groundmass composed of plagioclase, secondary quartz and calcite that occur as either interstitial or impregnation. The primary minerals

https://doi.org/10.1017/S001675681900150X

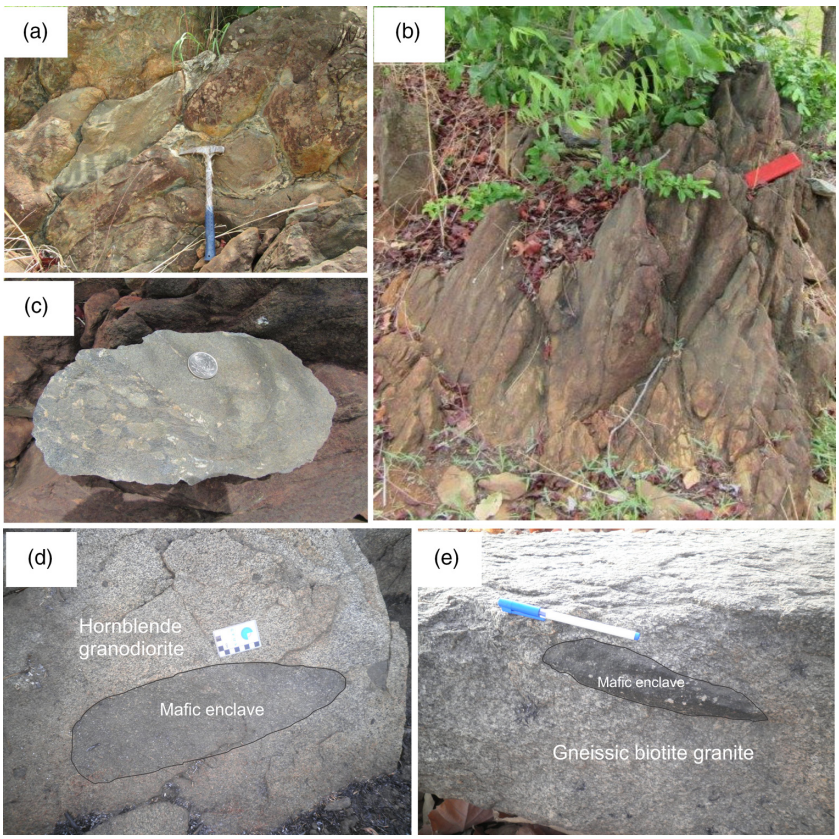

Fig. 2. (Colour online) Field outcrop photographs from the Lawra Volcanic Belt: (a) meta-basalt with preserved pillow structures near Jirapa; (b) an outcrop of meta-basalt (PAS 14) near Lawra; (c) hand specimen of basalt (PAS 13a) sampled from outcrop in Figure 3a; (d) mafic enclave (PAS 2b) in hornblende granodiorite (PAS 2a) near Wechiau; and (e) mafic enclave (PAS 31b) in gneissic biotite granite (PAS 31a), near Wa.

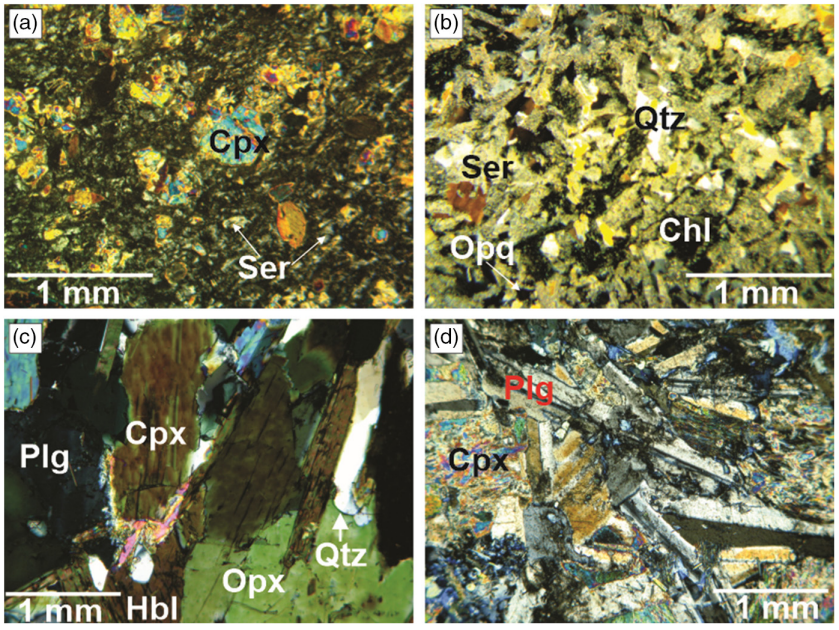

Fig. 3. (Colour online) Photomicrographs (crossed nicols) of the metavolcanic rocks and enclaves: (a) meta-andesite (Lawra); (b) meta-basalt (Lawra); (c) diorite enclave; (d) gabbro enclave. Cpx – clinopyroxene; Opx – orthopyroxene; Ser – sericite; Qtz – quartz; Opq – opaque; Chl – chlorite; Ep – epidote; Plg – plagioclase.

of the metabasalts (Fig. 3a) are mainly plagioclase (50–55%) and clinopyroxene (40–42%) that are either partially or completely replaced by actinolite and epidote. The plagioclase occurs as euhedral to subhedral phenocrysts, which are replaced partially or completely by epidote, actinolite and sericite, and to a lesser extent by albite and calcite. In some samples, relict clinopyroxene and plagioclase occur as subhedral to anhedral grains. Accessory minerals are apatite, magnetite and ilmenite.

The meta-andesites are greenish to dark grey, fine- to medium-grained, and massive to weakly foliated. They are porphyritic with plagioclase constituting the major phenocryst phase. As a result of metamorphism and alteration, some of the phenocrysts have been

https://doi.org/10.1017/S001675681900150X

replaced by actinolite, chlorite and epidote. For example, euhedral to subhedral plagioclase crystals are commonly replaced by epidote. The fine-grained groundmass is principally composed of plagioclase, and secondary actinolite, epidote and quartz. Apatite and opaque minerals occur as accessory minerals.

The amphibolite (PAS 20) is fine-grained, dark grey to green, and characterized by well-developed foliation. It is composed predominantly of hornblende and plagioclase with minor quartz. The fine-grained nature of the amphibolite suggests that its protolith was most likely to be basalt.

4.a.2. Granitoid-hosted enclaves

The enclaves are hosted mainly in hornblende granodiorite and gneissic biotite granite (detailed description in Sakyi *et al.* 2014), and are predominantly mafic in composition, made up of mainly diorites and gabbros. The only exceptions are samples PAS 7b and PAS 24, which are andesitic in composition. Some of the enclaves are either ellipsoidal or ovoid in shape and tend to have sharp contacts with the enclosing host rock (Fig. 2d, e). The diorite enclaves (Figs 2d, 3c) are dark grey, coarse-grained and weakly foliated, and are dominantly composed of plagioclase (25–20%), clinopyroxene and orthopyroxene (35–30%), hornblende (35–30%) with minor biotite (5%) and quartz (<5%). The plagioclase displays some degree of alteration, mostly in the core. The clinopyroxene is euhedral and occurs in elongated form and shows considerable degree of alteration. The biotite is tabular to bladed, while the hornblende is subhedral and sometimes altered to epidote. The gabbros (Figs 2e, 3d) are dark, medium- to coarse-grained and massive, and are principally composed of calcic plagioclase feldspar (60%) and clinopyroxene (35%) that are altered to sericite and chlorite, and epidote, respectively, but retain preserved pseudomorphs. Also present are chlorites (5%) and interstitial quartz, which shows undulose extinction.

4.b. Major- and trace-element geochemistry

4.b.1. Metavolcanic rocks

The whole-rock geochemical compositions of the metavolcanic samples are provided in Table 1. The samples have SiO_2 contents of 48.2–55.7 wt%, Al_2O_3 (8.20–16.3 wt%), Fe_2O_3T (6.74–15.2 wt%), MgO (2.80–14.7 wt%), CaO (4.85–12.9 wt%), Na_2O (0.37–4.04 wt%), K_2O (0.10–2.94 wt%) and TiO_2 (0.49–1.03 wt%). These samples also display a wide range of V, Cr, Ni and Co contents. The V content ranges over 115–312 ppm, Cr of 33.1–1174 ppm, Co of 16.9–63.5 ppm and Ni of 22.8–386 ppm. On the binary diagram of major oxide versus SiO_2 (Fig. 4), the metavolcanic rocks display trends of decreasing MgO, CaO, TiO_2 and Fe_2O_3T with progressive increase in SiO_2, while Na_2O and Al_2O_3 increase with increasing SiO_2 contents. K_2O and P_2O_5 do not produce any defined trend with SiO_2 (Fig. 4). The metavolcanics plot dominantly as tholeiites on both the K_2O versus SiO_2 and AFM ($Na_2O + K_2O$ – FeOt – MgO) diagrams (Fig. 5a, c) and partly as tholeiites on the Th versus Co diagram (Fig. 5b). The chondrite-normalized rare Earth element (REE) (Fig. 6a) and multi-element (Fig. 6b) patterns of the metavolcanic rocks conform well with normal mid-ocean-ridge basalt (N-MORB) -type magmatism. They contain higher REE concentrations compared with those of chondrite (Fig. 6a); however, from the chondrite-normalized REE diagram (Fig. 6a), four of the metavolcanic rocks show flat but parallel-to-subparallel patterns, with two samples showing light REE (LREE) enrichment and heavy REE (HREE) depletion, while one sample displays depletion in LREE relative to HREE. The samples define weak positive to negative Eu (Eu/Eu* = 0.90–1.14) anomalies. On the N-MORB-normalized diagram (Fig. 6b), the metavolcanic rocks display depletion in Rb, Th, Nb, Ta, Ti and P and enrichment in Ba, U, K and Sr. On the whole, they are enriched in large-ion lithophile elements (LILE) relative to N-MORB; however, their high-field-strength element (HFSE) and HREE concentrations are similar to those of N-MORB.

4.b.2. Granitoid-hosted enclaves

The geochemistry of the enclaves is presented in Table 2. The enclaves show significant variations in major-element content. For example, SiO_2 contents range from 48.6 to 68.9 wt%, suggestive of their evolved nature. Other oxides are Al_2O_3 (13.6–16.0 wt%), Fe_2O_3T (2.97–13.5 wt%), MgO (1.14–9.61 wt%), CaO (2.27–13.8 wt%), Na_2O (1.34–4.91 wt%), K_2O (0.13–2.67 wt%) and TiO_2 (0.50–0.81 wt%). The Ni contents of the enclaves range between 5.26 and 185 ppm, Co 5.54–47.8 ppm, Cr 8.06–492 ppm and V 36.2–168 ppm.

The enclaves generally contain higher values of Fe_2O_3T, MgO, CaO, MnO, Na_2O, TiO_2 and P_2O_5 transition elements (Ni, Cr, Co, V) and lower values of SiO_2, K_2O, Na_2O and Zr than their host (Sakyi *et al.* 2014, table 1), consistent with the occurrence of abundant ferromagnesian minerals in the enclaves. These further indicate the crystallization of the enclaves from more mafic magma.

In Figure 4, the enclaves define trends of decreasing MgO, CaO, TiO_2 and Fe_2O_3T with increasing SiO_2, whereas Na_2O and Al_2O_3 show positive correlation with SiO_2 contents. The plots of K_2O and P_2O_3 against SiO_2 do not produce any defined trend (Fig. 4). The enclaves plot mainly as calc-alkaline (Fig. 5a–c). They contain higher REE concentrations compared with those of chondrite, but they generally define enriched LREE patterns relative to HREE with pronounced Eu-negative (Eu/Eu* = 0.57–0.95) anomalies (Fig. 6c), except for one sample that defines a nearly flat REE pattern with weak Eu-positive (Eu/Eu* = 1.21) anomaly. Compared with N-MORB, the enclaves (with the exception of the HREE) are relatively enriched but display features of subduction-related magmatism (Fig. 6d). However, they display positive peaks in Ba, U, K and Sr and negative peaks in Rb, Nb, Ta, La, Ce, P and Ti. Generally, the enclaves have geochemical features that are similar to those of the metavolcanic rocks.

4.c. Sr–Nd isotope geochemistry

The Sr–Nd isotopic data, including $^{87}Sr/^{86}Sr$ initial ratios and $\varepsilon_{Nd}(T)$ and Nd model ages (T_{DM1} and T_{DM2}) for the metavolcanic rocks and enclaves are presented in Table 3. The initial $^{87}Sr/^{86}Sr$ ratios and ε_{Nd} values were calculated using an age of 2.1 Ga, representing crustal formation during the Eburnean Orogeny (e.g. Abouchami *et al.* 1990; Boher *et al.* 1992). The metavolcanic rocks and enclaves show low initial $^{87}Sr/^{86}Sr$ ratios ranging over 0.69868–0.70183 and 0.70126–0.70160, respectively (Table 3). The metavolcanics also show moderate to low positive ε_{Nd} values of +0.79 to +2.86, while the enclaves have low positive ε_{Nd} values of +0.79 to +1.82.

Crustal residence age (T_{DM}) of crustal rocks can be calculated by employing diverse models of depleted mantle evolution (e.g. DePaolo, 1981; Othman *et al.* 1984; Albarède & Brouxel, 1987; Liew & Hofmann, 1988; Blichert-Toft & Albarède, 1997). The Nd model age of crustal rocks indicates their time of extraction from the mantle. It is assumed that a Sm–Nd model age represents an average crustal residence time. However, this assumption is valid only if the crustal material has not experienced any

https://doi.org/10.1017/S001675681900150X

Table 1. Whole-rock major- and trace-element compositions of the Palaeoproterozoic Birimian metavolcanic rocks from the Lawra Volcanic Belt of Ghana

Sample no.	PAS 9	PAS 11	PAS 13a	PAS 14	PAS 20	PAS 21	PAS 22
Units: wt%							
SiO_2	48.2	48.7	50.1	55.7	50.5	50.7	55.7
Al_2O_3	11.4	8.20	13.9	16.3	12.0	14.7	12.1
Fe_2O_3T	11.7	12.7	11.4	6.74	15.2	12.1	11.1
CaO	9.24	11.6	10.8	4.85	9.87	11.0	12.9
MgO	14.7	13.9	9.22	2.80	7.20	6.60	3.77
MnO	0.17	0.19	0.17	0.09	0.23	0.17	0.16
Na_2O	0.85	0.84	1.94	4.04	3.00	2.01	0.37
K_2O	0.77	0.14	0.24	2.94	0.27	0.25	0.10
TiO_2	0.49	0.73	0.66	0.85	0.96	1.03	0.96
P_2O_5	0.04	0.06	0.05	0.38	0.08	0.09	0.11
LOI(%)	2.43	2.83	1.54	5.18	0.60	1.34	2.78
Total	99.9	99.9	100.0	100.0	100.0	100.0	100.0
Units: ppm							
Ba	133	26.3	83.5	1156	60.7	78.1	87.2
Rb	27.3	2.17	4.57	68.4	2.11	5.62	0.32
Sr	116	137	229	750	116	136	303
Y	10.0	12.8	13.1	15.9	26.0	22.7	24.3
Zr	29.0	35.3	35.0	139	53.5	52.5	72.7
Nb	1.24	1.72	1.53	5.69	1.75	2.27	2.77
Th	0.61	0.12	0.59	3.20	0.29	0.15	0.71
Pb	1.15	1.59	1.27	5.92	1.57	2.72	4.24
Ga	10.6	11.5	12.9	20.0	15.6	15.5	15.9
Zn	63.1	73.0	66.9	99.0	108	97.3	58.7
Cu	55.7	86.8	143	19.2	71.2	139	174
Ni	366	386	157	22.8	53.8	80.8	46.9
V	170	195	209	115	272	312	238
Cr	1174	1049	403	33.1	35.3	111	62.1
Hf	0.80	1.02	1.03	3.74	1.63	1.50	2.04
Cs	0.66	0.17	0.03	1.10	0.09	0.56	0.28
Ta	0.10	0.12	0.11	0.38	0.16	0.16	0.20
Co	63.5	63.3	51.1	16.9	57.9	61.7	36.8
U	0.20	0.01	0.19	0.94	0.09	0.07	0.24
Li	22.1	5.74	9.64	22.2	9.81	7.31	4.38
Be	0.22	0.24	0.18	1.17	0.33	0.26	0.35
Sc	34.6	30.8	38.1	11.7	50.3	45.1	39.9
Ti	2938	4377	3957	5096	5755	6175	5755
P	175	262	218	1659	349	393	480
K	6392	1162	1992	24406	2241	2075	830
La	3.38	0.78	3.21	29.8	2.80	3.02	7.12
Ce	5.83	3.26	6.89	64.6	6.96	8.24	16.2
Pr	0.87	0.70	1.06	8.06	1.22	1.30	2.21
Nd	3.94	4.12	5.21	33.6	6.27	6.73	10.2
Sm	1.16	1.59	1.55	6.09	2.19	2.18	2.63
Eu	0.47	0.58	0.58	1.68	0.77	0.85	0.87

(*Continued*)

https://doi.org/10.1017/S001675681900150X

Table 1. (*Continued*)

Sample no.	PAS 9	PAS 11	PAS 13a	PAS 14	PAS 20	PAS 21	PAS 22
Gd	1.36	1.82	1.83	4.97	3.13	2.96	3.33
Tb	0.29	0.39	0.37	0.66	0.65	0.58	0.64
Dy	1.88	2.52	2.48	3.31	4.59	3.94	4.19
Ho	0.40	0.55	0.54	0.63	1.04	0.87	0.93
Er	1.15	1.53	1.50	1.57	3.04	2.50	2.69
Tm	0.17	0.23	0.22	0.22	0.47	0.39	0.42
Yb	1.08	1.50	1.41	1.40	3.10	2.54	2.74
Lu	0.17	0.23	0.22	0.21	0.49	0.40	0.43

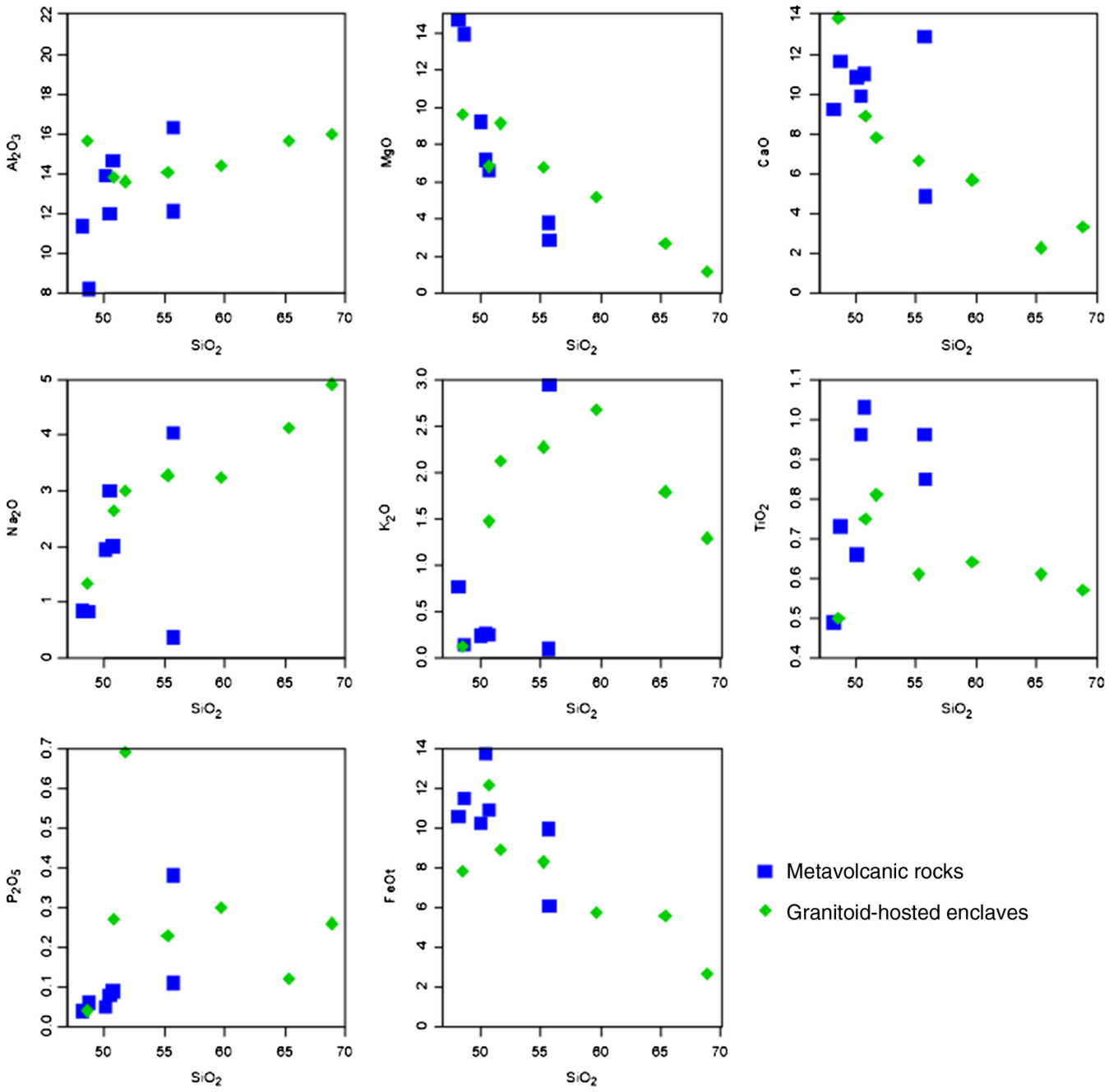

Fig. 4. (Colour online) Harker diagrams of rocks from the Lawra Volcanic Belt, showing the major elements plotted against SiO_2. Most of the major oxides display negative correlation with SiO_2.

https://doi.org/10.1017/S001675681900150X

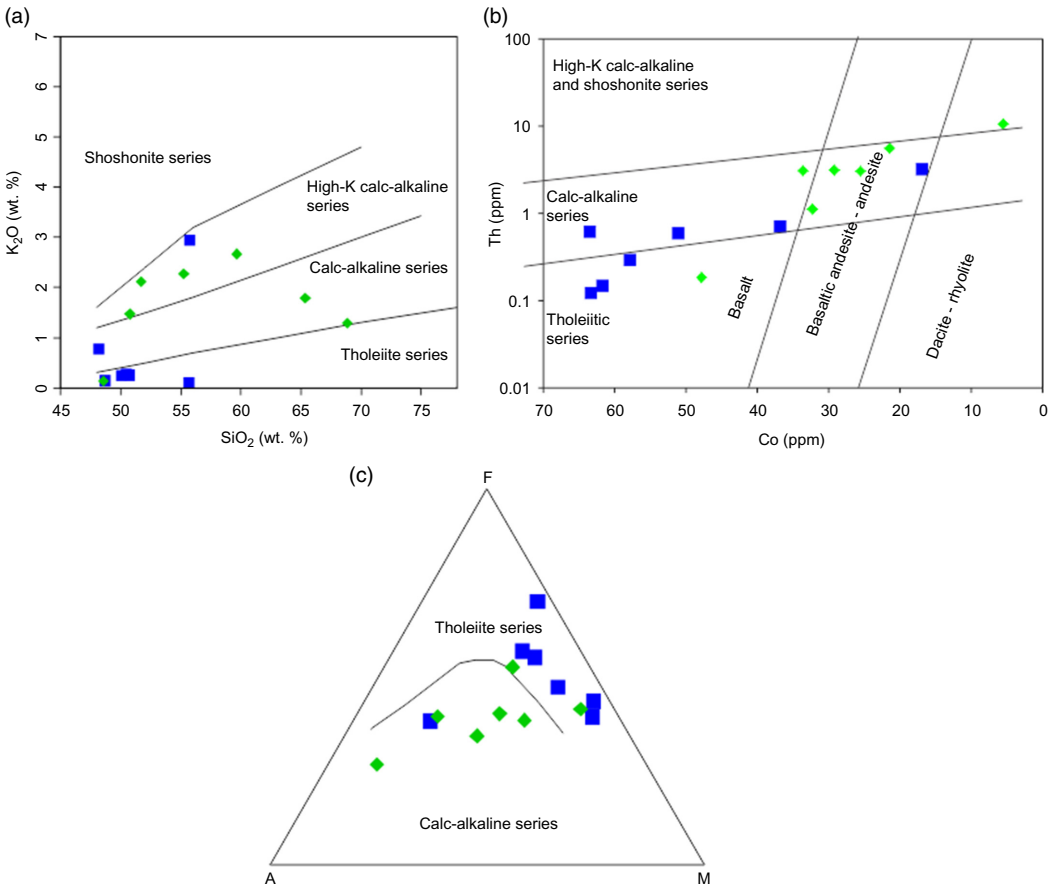

Fig. 5. (Colour online) (a) K_2O versus SiO_2; (b) Th–Co diagram of Hastie *et al.* (2007); and (c) AFM diagram of the Lawra metavolcanic rocks and enclaves (Irvine & Baragar, 1971). The samples plot within the respective calc-alkaline series, high-K calc-alkaline series and tholeiite series.

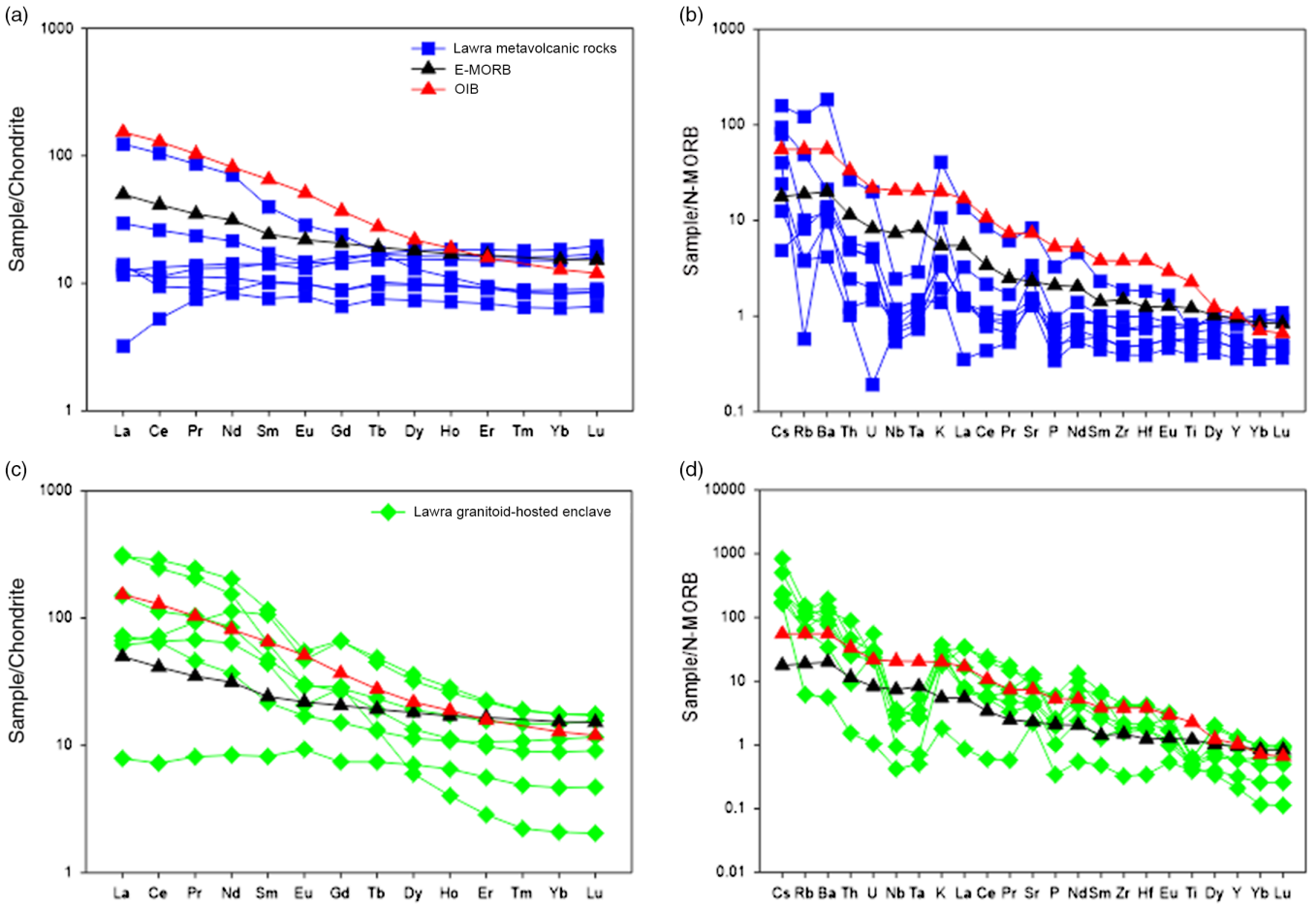

Fig. 6. (Colour online) (a, c) Chondrite-normalized REE and (b, d) N-MORB-normalized trace-element patterns for the rocks in the study area. Chondrite-normalizing values are from Boynton (1984), whereas N-MORB-normalizing values are from Sun & McDonough (1989). E-MORB and OIB data are from Gale *et al.* (2013).

https://doi.org/10.1017/S001675681900150X

Table 2. Whole-rock major- and trace-element compositions of granitoid-hosted enclaves from the Lawra Volcanic Belt of Ghana

Sample no.	PAS 17b	PAS 2b	PAS 31b	PAS 19	PAS 12b	PAS 7b	PAS 24
Units: wt%							
SiO_2	55.3	51.7	50.8	48.6	59.7	68.9	65.4
Al_2O_3	14.1	13.6	13.8	15.7	14.4	16.0	15.7
Fe_2O_3T	9.20	9.89	13.5	8.67	6.40	2.97	6.21
CaO	6.66	7.79	8.87	13.8	5.68	3.32	2.27
MgO	6.77	9.13	6.81	9.61	5.14	1.14	2.69
MnO	0.17	0.15	0.23	0.13	0.11	0.03	0.09
Na_2O	3.28	2.99	2.64	1.34	3.24	4.91	4.12
K_2O	2.27	2.12	1.47	0.13	2.67	1.29	1.79
TiO_2	0.61	0.81	0.75	0.50	0.64	0.57	0.61
P_2O_5	0.23	0.69	0.27	0.04	0.3	0.26	0.12
LOI(%)	1.37	1.12	0.89	1.54	1.63	0.65	1.07
Total	100.0	100.0	99.9	99.9	100.0	100.0	100.0
Units: ppm							
Ba	573	900	214	35.2	1214	773	482
Rb	85.9	57.6	34.4	3.45	67.6	36.7	57.9
Sr	404	706	442	196	1142	1002	375
Y	25.2	35.6	36.9	8.88	16.4	5.86	16.6
Zr	117	320	132	23.9	160	309	138
Nb	6.88	8.28	8.27	0.98	6.80	2.20	5.00
Th	3.13	3.08	1.12	0.18	5.57	10.6	3.04
Pb	12.3	7.34	9.19	0.99	14.1	10.0	9.59
Ga	18.2	21.8	24.1	14.7	19.4	21.6	15.9
Zn	117	120	193	46.1	81.1	68.1	69.9
Cu	43.0	48.3	81.5	144	24.7	16.2	11.2
Ni	73.5	142	74.1	185	63.0	5.26	85.5
V	144	168	168	157	124	36.2	122
Cr	378	492	395	230	239	8.06	166
Hf	3.54	8.61	4.11	0.70	4.39	8.16	3.68
Cs	5.83	1.58	1.63	1.16	1.69	1.23	3.51
Ta	0.73	0.35	0.37	0.07	0.47	0.09	0.35
Co	29.2	33.6	32.3	47.8	21.4	5.54	25.5
U	2.60	1.43	1.26	0.05	1.34	1.10	1.01
Li	52.0	29.4	19.4	6.94	19.9	34.3	48.4
Be	1.81	1.35	2.28	0.14	1.75	0.90	0.93
Sc	27.6	26.6	34.8	34.2	18.1	2.08	11.9
Ti	3657	4856	4496	2998	3837	3417	3657
P	1004	3012	1178	175	1310	1135	524
K	18844	17599	12203	1079	22165	10709	14859
La	14.8	73.1	16.1	1.91	36.1	75.4	17.5
Ce	40.6	178	44.5	4.49	69.9	152	40.2
Pr	6.36	23.0	8.74	0.77	9.74	19.3	4.34
Nd	30.1	95.7	53.6	3.98	40.1	73.0	17.4

(*Continued*)

https://doi.org/10.1017/S001675681900150X

Table 2. (*Continued*)

Sample no.	PAS 17b	PAS 2b	PAS 31b	PAS 19	PAS 12b	PAS 7b	PAS 24
Sm	6.74	17.8	16.4	1.26	7.29	9.80	3.34
Eu	1.22	3.23	2.76	0.55	1.78	1.71	1.00
Gd	5.82	13.8	13.6	1.54	5.47	5.98	3.12
Tb	0.89	1.72	1.85	0.28	0.72	0.51	0.49
Dy	4.86	8.19	9.17	1.80	3.43	1.53	2.91
Ho	0.98	1.46	1.61	0.37	0.64	0.23	0.61
Er	2.58	3.62	3.73	0.93	1.63	0.47	1.77
Tm	0.39	0.49	0.50	0.13	0.23	0.06	0.28
Yb	2.50	2.97	2.97	0.79	1.50	0.35	1.88
Lu	0.39	0.44	0.43	0.12	0.23	0.05	0.29

fractionation of Sm/Nd since the first separation of its protolith from the mantle source. As this is not always the case, and there is a need to avoid either overestimation or underestimation of one-stage Nd model ages, a two-stage Nd model age (T_{DM2}) can be calculated for the rocks. We therefore adopted the one-stage (T_{DM1}) and two-stage (T_{DM2}) models of DePaolo (1981). DePaolo (1981) argued that T_{CHUR} model ages are not reliable and usually miscalculate the true crustal formation ages, and that T_{DM} model ages represent much more accurate ages of crust formation. DePaolo (1981) also stated that the crust is derived from a depleted mantle with elevated Sm/Nd ratios ($\varepsilon_{Nd} > 0$) and not a "primitive" mantle source ($\varepsilon_{Nd} = 0$); crust formation ages should therefore be calculated relative to the depleted mantle.

The metavolcanic rocks yield T_{DM1} ages of 2.41–2.76 Ga (except for two samples that yield 4.03–4.28 Ga) and T_{DM2} ages of 2.31–2.47 Ga. The enclaves yield T_{DM1} and T_{DM2} ages of 2.37–2.46 Ga and 2.39–2.47 Ga, respectively (Table 3). Both one-stage and two-stage model ages have their own uncertainties (Dampare *et al.* 2008). According to Wu *et al.* (2005), more accurate results could be obtained for the single-stage model age if the Sm/Nd fractionation ($f_{Sm/Nd}$) is limited to the range −0.2 to −0.6. In this study, the $f_{Sm/Nd}$ values of the metavolcanic rocks range from −0.44 to +0.03; those for the enclaves range from −0.48 to −0.05. The inconsistency in the T_{DM1} ages for the metavolcanic rocks could therefore be explained by the above-mentioned fractionation effect, and these data were not considered further. The two-stage Nd model ages (T_{DM2}) also display a more consistent pattern compared with the single-stage model age (T_{DM1}); T_{DM2} ages will therefore be used in further discussions.

5. Discussion

5.a. Alteration and effects of weathering

The loss on ignition (LOI) values for the metavolcanic rocks and mafic enclaves are in the range of 0.60–5.18% and 0.65–1.63%, respectively (Tables 1, 2). These values are generally low, suggesting that the samples are relatively fresh. Previous studies have shown that the Birimian rocks have undergone metamorphism mostly under greenschist facies conditions (e.g. Sylvester & Attoh, 1992; Dampare *et al.* 2008; Amponsah *et al.* 2015, 2016*a*, *b*; Block *et al.* 2016*b*). Petrographic studies of the samples show that the primary mineral assemblages and textures have not experienced significant alteration. Regardless, we calculated the chemical index of alteration (CIA) (Nesbitt & Young, 1982) to determine the extent to which they have been altered by secondary processes. The CIA values obtained are 26.6–47.0 (average, 36.4) for the metavolcanic rocks and 36.4–55.2 (average, 43.8) for the enclaves. According to Nesbitt & Young (1982), the CIA value of unaltered rock is 50 and any CIA value exceeding 60 can be considered as significantly altered. This range of values suggests that the studied samples are relatively fresh and could therefore be relied upon for geochemical investigations. Similarly, the calc-alkaline to high-K calc-alkaline and tholeiite series signatures commonly displayed by the samples on the plots of K_2O versus SiO_2 (Fig. 5a; Peccerillo &Taylor, 1976) and transition versus fluid immobile elements (e.g. Co versus Th; Fig. 5b; Hastie *et al.* 2007) indicate that the LILE (e.g. K) were least affected by alteration and/or metamorphism. Although the alkali (e.g. K_2O and Na_2O) values may have been affected by alteration, the LOI and CIA values and inferences made from them strongly indicate they are relatively primary.

5.b. Petrogenesis of the metavolcanic rocks and enclaves

In Figure 5a–c the metavolcanic rocks display mainly tholeiite signatures, whereas the enclaves broadly display calc-alkalic signatures, a reflection of an evolved magma formed in an arc environment. Again, the SiO_2 contents of the samples (48.2–68.9 wt%) suggest that some of them are moderately evolved. The parallel to subparallel pattern displayed by the REEs (Fig. 6a, c) agrees with the interpretation that these samples have not undergone any significant fractionation.

The negative trends defined by decreasing CaO, Fe_2O_3T and MgO with increasing SiO_2 content (Fig. 4) indicate that plagioclase and olivine and/or pyroxene were probably the major phases that crystallized out during the evolution of the magma (Yücel *et al.* 2017). The effects of fractional crystallization on the composition of primary magma and partial melting are sometimes very difficult to differentiate. However, the plots of compatible and incompatible elements can be used to determine the processes that occurred during magma ascent (Dampare *et al.* 2008). This is because the fractionation of ferromagnesian minerals such as pyroxene and olivine

https://doi.org/10.1017/S001675681900150X

Table 3. Rb–Sr and Sm–Nd isotopic compositions of Palaeoproterozoic Birimian metavolcanic rocks and enclaves from the Lawra Volcanic Belt of Ghana. Source of TDM data: DePaolo (1981)

Sample	Rb (μg g^{-1})	Sr (μg g^{-1})	$^{87}Rb/^{86}Sr$	$^{87}Sr/^{86}Sr$	Error (2σ)	$(^{87}Sr/^{86}Sr)i$	Sm (μg g^{-1})	Nd (μg g^{-1})	$^{147}Sm/^{144}Nd$	$^{143}Nd/^{144}Nd$	Error (2σ)	ε_{Nd} (2.1 Ga)	f (Sm/Nd)	T_{DM1} (Ga)	T_{DM2} (Ga)
Metavolcanic rocks															
PAS 9	30.5	122	0.7240	0.720601	0.000010	0.698679	1.03	3.55	0.1746	0.51246	0.000007	2.46	−0.112	2.68	2.34
PAS 13a	4.29	230	0.0540	0.702955	0.000011	0.701322	1.31	4.42	0.1793	0.51254	0.000007	2.86	−0.088	2.67	2.31
PAS 14	74.3	785	0.2737	0.709644	0.000016	0.701353	5.60	30.6	0.1109	0.51152	0.000012	1.26	−0.436	2.41	2.43
PAS 20	3.12	120	0.0750	0.702887	0.000011	0.700611	2.08	6.18	0.2032	0.51285	0.000009	2.43	0.033	4.28	2.34
PAS 21	6.46	136	0.1380	0.704863	0.000013	0.700704	2.12	6.56	0.1953	0.51266	0.000007	0.79	−0.007	4.03	2.47
PAS 22	0.97	306	0.0092	0.702109	0.000010	0.701831	2.55	9.61	0.1603	0.51218	0.000007	0.83	−0.185	2.76	2.47
Mafic enclaves															
PAS 12b	67.6	1165	0.1678	0.706681	0.000014	0.701600	6.47	35.4	0.1105	0.51154	0.000027	1.82	−0.438	2.37	2.39
PAS 17a	86.0	656	0.3790	0.712748	0.000009	0.701261	3.37	19.9	0.1026	0.51141	0.000008	1.51	−0.478	2.37	2.41
PAS 31b	34.1	433	0.2279	0.708205	0.000011	0.701308	14.5	46.9	0.1875	0.51255	0.000007	0.79	−0.047	3.46	2.47

decreases the concentrations of compatible elements (e.g. Ni and Cr) and increases the concentration of incompatible elements (e.g. Th, La and Nd) in the liquids (Dampare *et al.* 2008). On the plot of Ni (compatible element) and Th (incompatible element) versus SiO_2 (Fig. 7a, b), there is a decrease in Ni and slight increase in Th with increasing SiO_2 content. This suggests that the metavolcanic rocks and enclaves might have undergone minor fractional crystallization during their evolution (Dampare *et al.* 2008). The decrease in Ni content with increasing SiO_2 content indicates that olivine was probably the primary phase that fractionated out of the melt (Yücel *et al.* 2017).

Constant Th/Nb and Nb/Yb values are characteristics of basaltic rocks derived from the mantle lithosphere, the plume asthenosphere or depleted MORB mantle. In a plot of Th/Yb versus Nb/Yb, such basaltic rocks usually plot in or around the diagonal mantle array (Pearce, 1983, 2014; Pearce & Peate, 1995). In the plot of Th/Yb versus Nb/Yb discrimination diagram, after Pearce (1983) (Fig. 8), all the samples display high Th/Yb ratios relative to that of the mantle array, with all but two of the metavolcanics samples plotting above the N-MORB/ocean island basalt (OIB) array. One enclave sample, with a Th/Yb value of 30, falls outside the range of values for the plot. The trend displayed by the metavolcanic rocks and the enclaves suggests arc-related magmatism (Pearce, 2008). Subduction-zone-related fluids often entrain Th relative to Nb, Ta or Yb, which signifies that Th, rather than Nb or Ta, would be enriched in source components that have been metasomatized by subduction processes, resulting in elevated Th/Yb ratios relative to Nb/Yb or Ta/Yb. Equally, crustal rocks are characterized by higher contents of Th compared to Nb and Ta. The higher Th/Yb values for both the enclaves and metavolcanic rocks may therefore indicate crustal assimilation during the evolution of the magma, or may be attributed to the enrichment of the mantle (source region) by a subducted component carrying Th but not Ta or Yb (Pearce *et al.* 1990). Our results are consistent with the latter process.

The metavolcanic rocks and enclaves display low initial $^{87}Sr/^{86}Sr$ ratios of 0.698679–0.701831 and 0.701261–0.701600, respectively. Earlier studies on Birimian rocks in Ghana and the rest of West Africa (e.g. Abouchami *et al.* 1990; Boher *et al.* 1992; Taylor *et al.* 1992; Gasquet *et al.* 2003; Dampare *et al.* 2009) have produced a wide range of initial $^{87}Sr/^{86}Sr$ ratios, ranging from as low as 0.65300 to 0.70623. The values obtained in this study fall within the range of values in previous studies, indicating that low $(^{87}Sr/^{86}Sr)i$ is typical of Birimian rocks in West Africa. Gasquet *et al.* (2003) and Dampare *et al.* (2009) attributed the low initial $^{87}Sr/^{86}Sr$ ratios to feldspar alteration and metamorphism. Petrographic observation of our samples further revealed that the feldspars are partially or wholly altered to sericite, epidote and calcite. We therefore do not place too much emphasis on the $(^{87}Sr/^{86}Sr)i$ ratio in our discussion. The positive ε_{Nd} (2.1 Ga) values of +0.79 to +2.86 for the metavolcanic rocks and +0.79 to +1.82 for the enclaves support the role of juvenile components in their genesis, indicating the significant input of new mantle-derived magmas. The juvenile nature of the samples is established in Figure 9a, where they plot close to the depleted mantle curve and are also widely separated from the Nd isotopic evolutionary trend of Archean crust. The positive ε_{Nd} values for some of the rocks suggest their derivation from a depleted mantle source (Srivastava *et al.* 2009). The range of initial ε_{Nd} values from our samples strongly suggests that the rocks were produced entirely from the mantle in an oceanic setting (DePaolo, 1988), with possible minor crustal contamination.

https://doi.org/10.1017/S001675681900150X

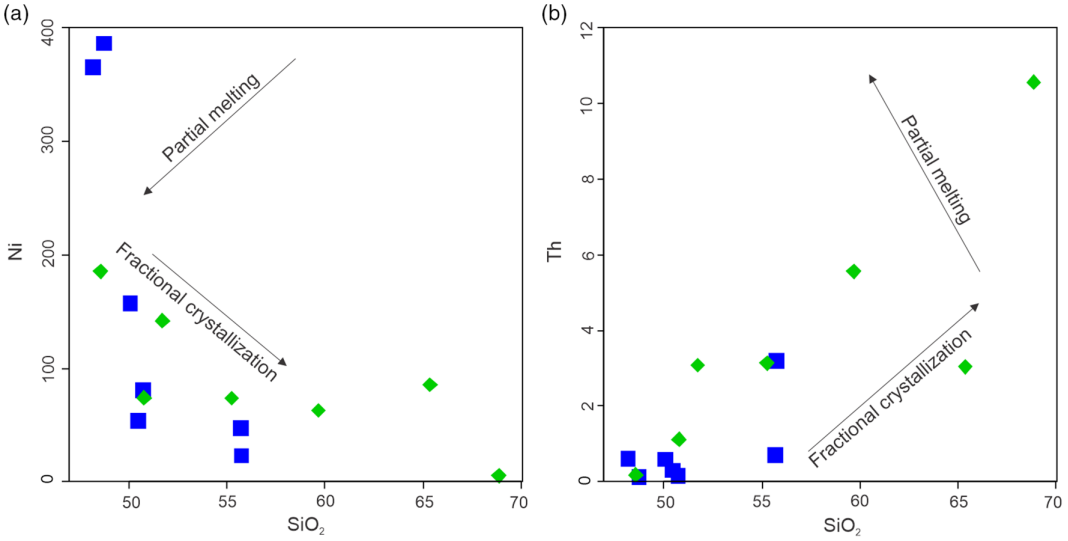

Fig. 7. (Colour online) Trace-element variations with respect to SiO_2 for the Lawra metavolcanic rocks and enclaves: (a) compatible element (Ni) variation with SiO_2; and (b) incompatible element (Th) variation with SiO_2.

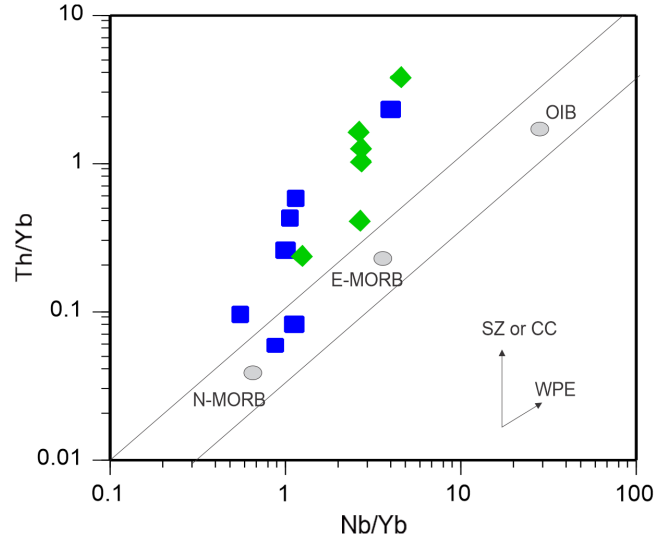

Fig. 8. (Colour online) Th/Yb versus Nb/Yb diagram (after Pearce, 1983; Pearce & Peate, 1995) of the metavolcanic rocks and enclaves. WPE – within-plate enrichment; SZ – subduction zone flux; CC – crustal contamination. N-MORB, E-MORB and OIB values from Sun & McDonough (1989).

In Figure 9b, the samples plot almost exclusively within the field defined by Birimian basalts and granitoids and this, coupled with the low and restricted $(^{87}Sr/^{86}Sr)_i$ values and low positive initial $\varepsilon_{Nd}(T)$ values, suggests that the metavolcanic rocks and enclaves have isotopic characteristics similar to rocks from other Birimian terranes in Ghana and West Africa (e.g. Abouchami *et al.* 1990; Boher *et al.* 1992; Taylor *et al.* 1992; Gasquet *et al.* 2003; Dampare *et al.* 2009). The Birimian basins and belts are intruded by different generations of granitoids (e.g. Agyei Duodu *et al.* 2009; Sakyi *et al.* 2014; Block *et al.* 2016*a*). However, the granitoid-hosted enclaves display an identical composition to that of the metavolcanic rocks. The mineralogical and geochemical features of the enclaves and metavolcanics support the idea that the granitoid rocks developed through variable degrees of mixing/mingling between a basic magma and granitic melt during subduction, when blobs of basic to intermediate parental magma became trapped in the granitic magma (Hassen *et al.* 2008; Rajaieh *et al.* 2010). The gabbro and andesite enclaves most likely represent the nearest composition to the original, more basic, magma.

The two-stage (T_{DM2}) Nd model ages of 2.31–2.47 Ga for the metavolcanic rocks and 2.39–2.47 Ga for the enclaves are higher than the formation age of 2.1 Ga, suggesting that they may have received some inputs from older crustal sources. However, the trace-element data of the studied samples are not consistent with crustal contamination. For example, the negative Nb–Ta anomalies could be attributed to crustal contamination; however, the negative Zr–Hf anomalies displayed by the rocks are inconsistent with crustal contamination, since crustal materials are enriched in elements such as Th, Zr and Hf. Since negative Zr–Hf anomalies are uncommon among intraplate basalts (Zhou *et al.* 2002), we ascribe the Nb–Ta and Zr–Hf depletions to a lack of an OIB component in the source region of the rocks. The metavolcanic rocks and enclaves may therefore have been derived from lithospheric mantle sources.

Several recent studies have revealed the existence of older crustal materials in parts of the WAC. For example, SHRIMP U–Pb geochronological studies on zircons from granitoids in the Bolé–Wa region of NW Ghana (de Kock *et al.* 2011) produced inherited ages of 2876 and 2499 Ma, showing that continental crust was involved until the generation of the Gondo granite within the Bolé–Navrongo Belt. Petersson *et al.* (2016) conducted zircon U–Pb age dating and Lu–Hf isotopic systematics on granitoids from southern Ghana, and revealed zircon with an $^{207}Pb/^{206}Pb$ age of 2460 Ma, interpreted to be of xenocrystic origin. Similarly, *in situ* zircon U–Pb dating and Lu–Hf isotope analyses carried out on inherited zircons in granitoids from northern Ghana yielded ages of 2220–2360 Ma (Block *et al.* 2016*a*). Parra-Avila *et al.* (2019) inferred that the eastern part of the Baoulé–Mossi domain is underlain by Archean rocks, giving rise to predominately older ages (*c.* > 2100 Ma). Thiéblemont *et al.* (2001) recorded U–Pb ages of 3542 and 3535 Ma for the granite–gneiss association in the Archean Kenema–Man domain of Guinea, and the late Eburnean plutonic belt of eastern Guinea is a key element of the Archean–Proterozoic transition zone in the southern part of West Africa (Egal *et al.* 2002).

https://doi.org/10.1017/S001675681900150X

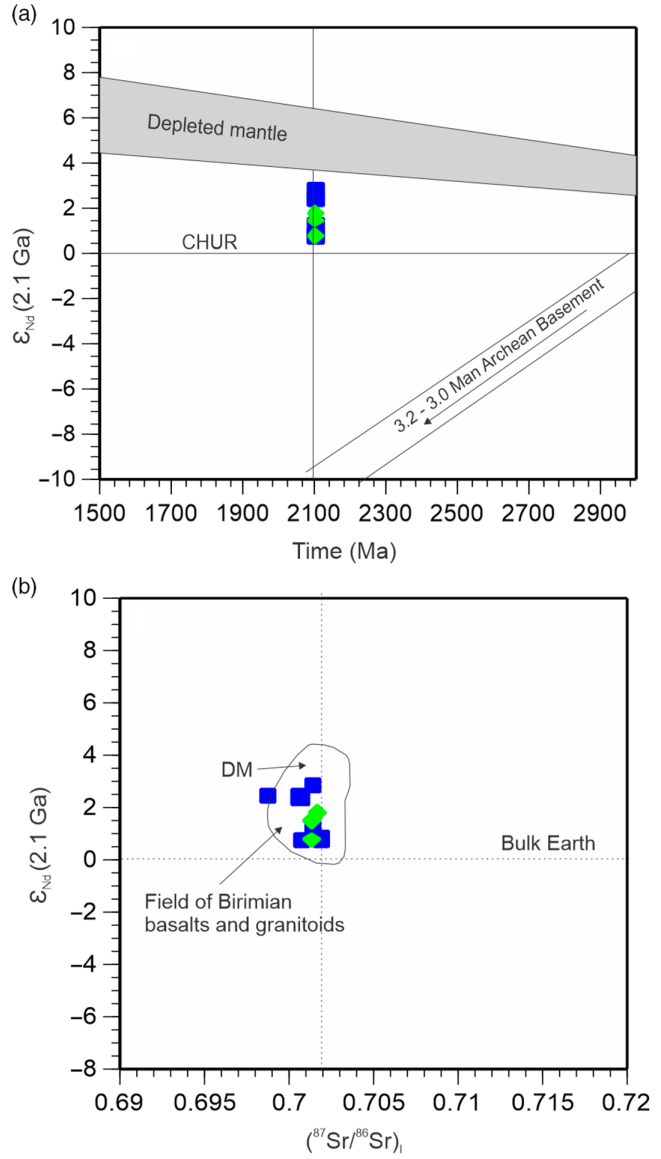

Fig. 9. (Colour online) (a) Plot of ε_{Nd} (2.1 Ga) versus formation age (time) for the Palaeoproterozoic metavolcanic rocks and enclaves from the study area. Data for Archean continental crust are from Kouamelan *et al.* (1997). (b) ε_{Nd} (2.1 Ga) versus initial $^{87}Sr/^{86}Sr$ ratios (calculated at 2.1 Ga) plot for the Palaeoproterozoic metavolcanic rocks and mafic enclaves from the study area. Also shown is the field of isotopic composition of Birimian basaltic and felsic rocks (shaded area) from the WAC (adapted from Pawlig *et al.* 2006). DM represents contemporaneous depleted mantle from Othman *et al.* (1984).

Additionally, a Sm–Nd model age of *c.* 2600 Ma was obtained from Winneba granitoids in Ghana (Taylor *et al.* 1992). More recently, Petersson *et al.* (2016) obtained Hf model ages of 2.4–2.7 Ga for granites from southern and southwestern Ghana. Also, a recent study based on Lu–Hf isotopic systematics revealed that the crust of the western Baoulé–Mossi domain has Hf model ages of 2.80 Ga, indicating possible reworking of older crust in parts of the WAC (Parra-Avila *et al.* 2016). Similarly, Block *et al.* (2016*a*) produced two-stage Hf model ages of 2.35–2.61 Ga in zircons from granitoids of the Bole–Bulenga, Abulembire, Bawku and Koudougou–Tumu domains in northern Ghana. The abovementioned studies provide strong evidence that the Palaeoproterozoic Birimian Terrane of the WAC is underlain by Archean rocks. The model ages obtained here therefore support the juvenile character of the rocks, with the contribution of subducted pre-Birimian rocks (or Archean?) in the source material. We propose that magma for the studied rocks was derived from mantle source(s) modified by subducted materials.

5.c. Tectonic setting of the metavolcanic rocks and enclaves

Previous studies of the Palaeoproterozoic rocks have proposed different models to explain the tectonic setting of the rocks; namely the island-arc setting (Sylvester & Attoh, 1992; Béziat *et al.* 2000; Attoh *et al.* 2006; Feybesse *et al.* 2006; Dampare *et al.* 2008) and plume-related setting (e.g. Abouchami *et al.* 1990; Lompo, 2009). From the petrographic analyses, we observed that the rocks have undergone various degrees of alteration. It has also been reported in the literature (e.g. Hirdes *et al.* 1992; Attoh *et al.* 2006) that rocks of the Palaeoproterozoic Birimian have undergone greenschist facies metamorphism. These processes and alterations affect the distribution of the LILE and mean that the application of most major-element oxides and LILE for identifying tectonic setting of the metavolcanic rocks and enclaves is unreliable. Accordingly, the more resistant HFSE, including Nb, Zr, Ti, Y, Sr, La, Hf, Ta and Yb, have been used in determining the tectonic setting of the samples (Girty *et al.* 1994).

The metavolcanic rocks and enclaves (Tables 1, 2) have very low TiO_2 (<2.0 wt%) and are therefore inferred to represent igneous rocks from magmatic arcs (Pearce, 2014), which typically have low TiO_2. On the spider diagrams (Fig. 6b, d), the metavolcanic rocks and enclaves are characterized by positive Ba and Th anomalies and negative Nb–Ta, Zr–Hf and Ti anomalies, which are geochemical features that may connote the formation of the rocks in an arc setting (Fitton *et al.* 1988; Saunders *et al.* 1988). Our data therefore suggest subduction-related magmatism, and are consistent with an island-arc setting (Sylvester & Attoh, 1992; Béziat *et al.* 2000; Attoh *et al.* 2006; Dampare *et al.* 2008) rather than the proposed plume-generated setting (e.g. Abouchami *et al.* 1990) for the Palaeoproterozoic rocks of West Africa.

The tectonic setting of the metavolcanic rocks and enclaves was investigated using the tectonic discrimination diagram of Wood (1980) (Fig. 10a). On this diagram, the samples plot in the fields of calc-alkaline basalts (CAB), island-arc tholeiites (IAT) and N-MORB, supporting the interpretation that they were derived from an arc environment. The relative ratio of V and Ti can also be used to discriminate the tectonic environment of different types of basalts as proposed by Shervais (1982). In Figure 10b, the samples fall within the CAB–MORB–volcanic-arc basalt (VAB) overlap field, also indicating possible subduction-related magmatism. Further, on the plot of $f_{Sm/Nd}$ versus ε_{Nd} (2.1 Ga) (Fig. 10c), our samples plot almost exclusively within the field defined by arc rocks. This is consistent with the major- and trace-element data and supports the arc setting for the metavolcanic rocks and enclaves.

6. Conclusion

We have determined the petrography, geochemical and Sr–Nd isotope compositions of mafic metavolcanic rocks and mafic enclaves from the Palaeoproterozoic Lawra Belt in Ghana. The following conclusions can be made from our study.

https://doi.org/10.1017/S001675681900150X

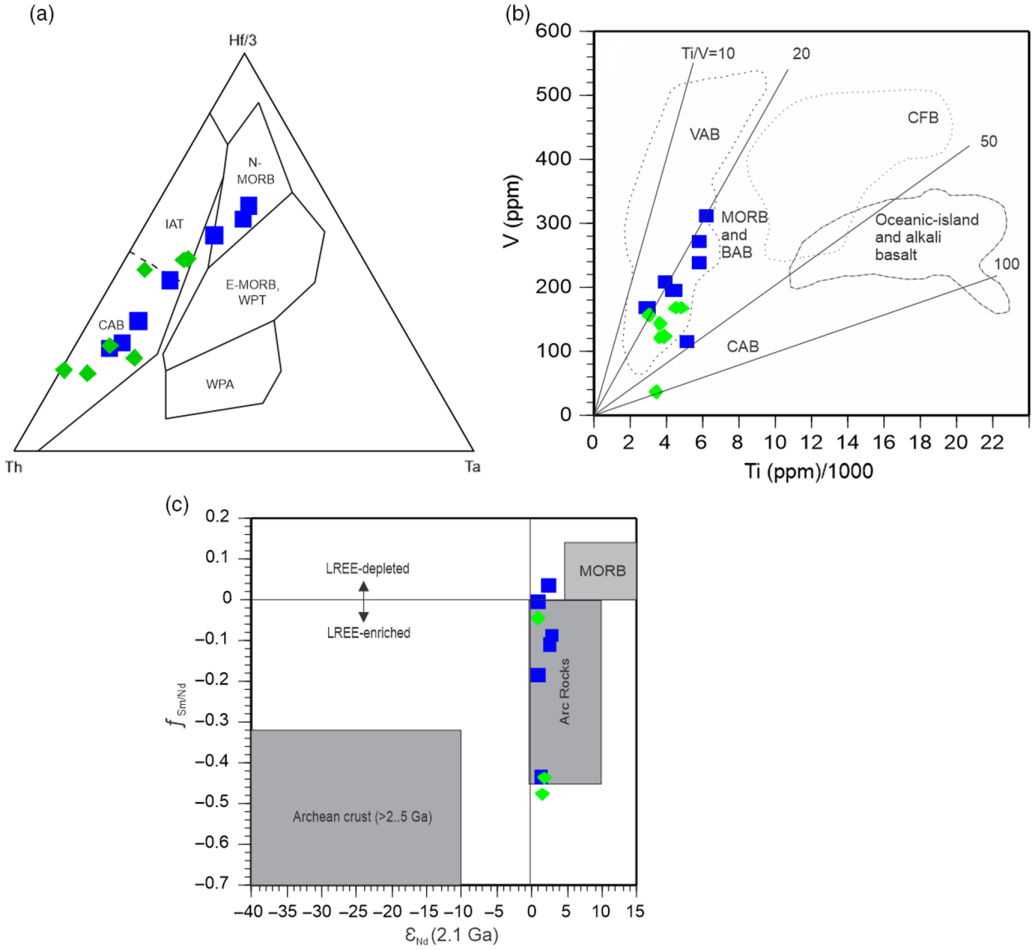

Fig. 10. (Colour online) Discriminant diagrams indicating tectonic settings for the studied metavolcanic rocks and enclaves: (a) Hf–Th–Ta by Wood (1980), (b) V versus Ti plot of Shervais *et al.* (1982); and (c) plot of ε_{Nd} (2.1 Ga) versus fractionation parameter ($f_{Sm/Nd}$) for the metavolcanic rocks and enclaves from the study area. Fields of old (Archean) continental crust, MORB and the arc rocks are from Roddaz *et al.* (2007), defining the tectonic setting of the studied rocks.

- The metavolcanic rocks are mainly meta-basalts and meta-andesites, while the enclaves are diorites and gabbros. Generally, the metavolcanic rocks and enclaves display identical geochemical and isotopic signatures, suggesting their derivation from the same source.
- The host granitoids developed through mixing/mingling between a basic magma and granitic melt, during which globules of basic to intermediate parental magma got trapped in the granitic magma.
- The very low TiO_2 (<2.0 wt%), pronounced Nb–Ta troughs, enrichment in Ba and Th as well as depletion of Ti of the metavolcanic rocks and enclaves are characteristic of subduction-related magmatism; these characteristics therefore indicate formation in an arc setting. The metavolcanic rocks and enclaves plot in the overlapping field CAB–IAT–N-MORB, also indicating possible subduction-related magmatism. The $f_{Sm/Nd}$ versus ε_{Nd} diagram shows that the samples plot almost exclusively within the field defined by arc rocks. All these support the arc affinity for the metavolcanic rocks and enclaves.
- The metavolcanic rocks and enclaves are represented by low ($^{87}Sr/^{86}Sr$)i values of 0.69868–0.70183 and 0.70126–0.70160, respectively, a typical characteristic of Birimian rocks in Ghana and the rest of West Africa. This signature is ascribed to feldspar alteration. The rocks also show positive ε_{Nd} values of +0.79 to +2.86 for the metavolcanic rocks and +0.79 to +1.82 for the enclaves, all indicating that the Birimian crust was most likely formed from juvenile mantle-derived magmas. On a plot of Th/Yb versus Nb/Yb, the rocks show high Th/Yb ratios relative to that of the mantle array, suggesting possible crustal contamination of these rocks.
- The Nd model ages (T_{DM2}) of 2.31–2.47 Ga for metavolcanic rocks and 2.39–2.47 Ga for the enclaves support the juvenile character of the rocks with a contribution from subducted pre-Birimian rocks (or Archean?) in the source material.
- The metavolcanic rocks and enclaves of the WAC in northwestern Ghana could be interpreted to have been formed in a common island-arc setting.

Acknowledgements. We thank Dr Solomon Anum of the Ghana Geological Survey Authority, Accra, for providing logistical support and help during fieldwork. We are grateful to Xindi Jin, Ding-Shuai Xue and Wenjun Li of the Institute of Geology and Geophysics, Chinese Academy of Sciences, for the elemental analyses. This study was financially supported by the National Natural Science Foundation of China (Grants 41772055 and 91755205) and State Key Laboratory of Lithospheric Evolution (Grant 201701) made available to BXS.

Declaration of Interest. None.

References

Abitty EK, Dampare SB, Nude PM and Asiedu DK (2016) Geochemistry and petrogenesis of the K-rich 'Bongo-type' granitoids in the Paleoproterozoic Bole-Nangodi greenstone belt of Ghana. *Journal of African Earth Sciences* **122**, 47–62.

Abouchami W, Boher M, Michard A and Albarede F (1990) A major 2.1 Ga old event of mafic magmatism in West Africa: an early stage of crustal accretion. *Journal of Geophysical Research* **95**, 17605–29.

Agyei Duodu J, Loh GK, Boamah KO, Baba M, Hirdes W, Toloczyki M and Davis DW (2009) *Geological Map of Ghana 1:1 000 000*. Accra: Geological Survey Department of Ghana (GSD).

Albarède F and Brouxel M (1987) The Sm–Nd secular evolution of the continental crust and the depleted mantle. *Earth and Planetary Science Letters* **82**, 25–35.

Amponsah PA, Salvi S, Béziat D, Baratoux L, Siebenaller L, Jessell M, Nude PM and Gyawu EA (2016a) Multistage gold mineralization in the Wa-Lawra greenstone belt, NW Ghana: the Bepkong deposit. *Journal of African Earth Sciences* **120**, 220–37.

Amponsah PA, Salvi S, Béziat D, Baratoux L, Siebenaller L, Nude PM, Nyarko RS and Jessell MW (2016b). The Bepkong gold deposit, Northwestern Ghana. *Ore Geology Reviews* **78**, 718–23.

Amponsah PA, Salvi S, Béziat D, Siebenaller L and Jessell MW (2015). Geology and geochemistry of the shear-hosted Julie gold deposit, NW Ghana. *Journal of African Earth Sciences* **112**, 505–23.

Anum S, Sakyi PA, Su BX, Nude PM, Nyame F, Asiedu D and Kwayisi D (2015) Geochemistry and geochronology of granitoids in the Kibi-Asamankese area of the Kibi-Winneba volcanic belt, southern Ghana. *Journal of African Earth Sciences* **102**, 166–79.

Asiedu DK, Asong S, Atta-Peters D, Sakyi PA, Su BX, Dampare SB and Anani CY (2017) Geochemical and Nd-isotopic compositions of juvenile-type Paleoproterozoic Birimian sedimentary rocks from southeastern West African Craton (Ghana): constraints on provenance and tectonic setting. *Precambrian Research* **300**, 40–52.

Asiedu DK, Dampare SB, Sakyi PA, Banoeng-Yakubo B, Osae S, Nyarko BJB and Manu J (2004) Geochemistry of Paleoproterozoic metasedimentary rocks from the Birim diamondiferous field, southern Ghana: implications for provenance and crustal evolution at the Archean-Proterozoic boundary. *Geochemical Journal* **38**, 215–28.

Attoh K, Evans MJ and Bickford ME (2006) Geochemistry of an ultramafic rodingite rock association in the paleoproterozoic dixcove greenstone belt, southwestern Ghana. *Journal of African Earth Sciences* **45**, 333–46.

Baratoux L, Metelka V, Naba S, Jessell MW, Gregoire M and Ganne J (2011) Juvenile Paleoproterozoic crust evolution during the Eburnean orogeny (~2.2–2.0 Ga), Western Burkina Faso. *Precambrian Research* **191**, 18–45.

Béziat D, Bourges F, Debat P, Lompo M, Martin F and Tollon F (2000) A Paleoproterozoic ultramafic-mafic assemblage and associated volcanic rocks of the Boromo greenstone belt: fractionates originating from island-arc volcanic activity in the West African craton. *Precambrian Research* **101**, 25–47.

Blichert-Toft J and Albarède F (1997) The Lu–Hf geochemistry of chondrites and the evolution of the mantle-crust system. *Earth and Planet Science Letters* **148**, 243–58.

Block S, Baratoux L, Zeh A, Laurent O, Bruguier O, Jessell M, Aillères L, Sagna R, Parra-Avila LA and Bosch D (2016a) Paleoproterozoic juvenile crust formation and stabilisation in the south-eastern West African Craton (Ghana); new insights from U-Pb-Hf zircon data and geochemistry. *Precambrian Research* **287**, 1–30.

Block S, Ganne J, Baratoux L, Zeh A, Parra-Avila LA, Jessell M, Aillères L and Siebenaller L (2015) Petrological and geochronological constraints on lower crust exhumation during Paleoproterozoic (Eburnean) orogeny, NW Ghana, West African Craton. Petrological and geochronological constraints on lower crust exhumation during Paleoproterozoic (Eburnean) orogeny, NW Ghana, West African Craton. *Journal of Metamorphic Geology* **33**, 463–94.

Block S, Jessell M, Aillères L, Baratoux L, Bruguier O, Zeh A, Bosch D, Caby R and Mensah E (2016b) Lower crust exhumation during Paleoproterozoic (Eburnean) orogeny, NW Ghana, West African Craton: interplay of coeval contractional deformation and extensional gravitational collapse. *Precambrian Research* **274**, 82–109.

Boher M, Abouchami W, Michard A, Albarède F and Arndt NT (1992) Crustal growth in West Africa at 2.1 Ga. *Journal of Geophysical Research* **95**, 345–69.

Boynton WV (1984) Geochemistry of rare earth elements: meteorite studies. In *Rare Earth Element Geochemistry* (ed. P Henderson), pp. 63–114. New York: Elsevier.

Chu ZY, Wu FY, Walker RJ, Rudnick RL, Pitcher L, Puchtel IS, Yang YH and Wilde SA (2009) Temporal evolution of the lithospheric mantle beneath the eastern North China Craton. *Journal of Petrology* **50**, 1857–98.

Dampare S, Shibata T, Asiedu D and Osae H (2005) Major-element geochemistry of Proterozoic Prince's Town granitoid from the southern Ashanti volcanic belt, Ghana. *Okayama University Earth Science Report* **12**, 15–30.

Dampare SB, Shibata T, Asiedu DK, Osae S and Banoeng-Yakubo B (2008) Geochemistry of Paleoproterozoic metavolcanic rocks from the southern Ashanti volcanic belt, Ghana: petrogenetic and tectonic setting implications. *Precambrian Research* **162**, 403–23.

Dampare S, Shibata T, Asiedu D, Osamu O, Manu J and Sakyi P (2009) Sr-Nd isotopic compositions of paleoproterozoic metavolcanic rocks from the southern Ashanti volcanic belt, Ghana. *Okayama University Earth Science Report* **16**, 9–28.

Davis DW, Hirdes W, Schaltergger U and Nunoo EA (1994) U-Pb age constraints on deposition and provenance of Birimian and gold-bearing Tarkwaian sediments in Ghana, West Africa. *Precambrian Research* **67**, 89–107.

de Kock GS, Armstrong RA, Siegfried HP and Thomas E (2011) Geochronology of the Birim Supergroup of the West African Craton in the Wa-Bolé region of west-central Ghana: implications for the stratigraphic framework. *Journal of African Earth Sciences* **59**, 1–40.

de Kock GS, Theveniaut H, Botha PW and Gyapong W (2009) Geological map explanation, map sheet 0803B (1:100,000). CGS/BRGM/Geoman. Accra, Ghana: Ghana Geological Survey Department.

DePaolo DJ (1981) Neodymium isotopes in the Colorado front range and crust-mantle evolution in the proterozoic. *Nature* **291**, 193–6.

DePaolo DJ (1988) *Neodymium Isotope Geochemistry: An Introduction*. Berlin: Springer, 187 p.

Doumbia S, Pouclet A, Kouamelan A, Peucat JJ, Vidal M and Delor C (1998) Petrogenesis of juvenile-type Birimian (Paleoproterozoic) granitoids in Central Côte d'Ivoire, West Africa: geochemistry and geochronology. *Precambrian Research* **87**, 33–63.

Egal E, Thiéblemont D, Lahondére D, Guerrot C, Costea CA, Iliescu D, Delor C, Goujou J-C, Lafon JM, Tegyey M, Diaby S and Kolie O (2002) Late Eburnean granitization and tectonics along the western and northwestern margin of the Archean Kénéma–Man domain (Guinea, West African Craton). *Precambrian Research* **117**, 57–84.

Eisenlohr B and Hirdes W (1992) The structural development of the early Proterozoic Birimian and Tarkwaian rocks of southwest Ghana, West Africa. *Journal of African Earth Sciences* **14**, 313–25.

Feybesse JL, Billa M, Guerrot C, Duguey E, Lescuyer JL, Milési JP and Bouchot V (2006) The Paleoproterozoic Ghanaian province: geodynamic model and ore controls, including regional stress modeling. *Precambrian Research* **149**, 149–96.

Feybesse JL and Milési JP (1994) The Archaean/Proterozoic contact zone in West Africa: a mountain belt of decollement thrusting and folding on a continental margin related to 2.1 Ga convergence of Archaean cratons? *Precambrian Research* **69**, 199–227.

Fitton JG, James D, Kempton PD, Ormerod DS and Leeman WP (1988) The role of lithospheric mantle in the generation of Late Cenozoic basic magmas in the Western United States. *Journal of Petrology* Special Volume, 331–49.

Gale A, Dalton CA, Langmuir CH, Su YJ and Schilling J-G (2013) The mean composition of ocean basalts. *Geochemistry, Geophysics, Geosystems* **14**, 489–518.

Ganne J, de Andrade V, Weinberg RF, Vidal O, Dubacq B, Kagambega N, Naba S, Baratoux L, Jessell M and Allibon J (2012) Modern-style plate subduction preserved in the Palaeoproterozoic West African Craton. *Nature Geoscience* **5**, 60–5.

Gasquet D, Barbey P, Adou M and Paquette JL (2003) Structure, Sr–Nd isotope geochemistry and zircon U-Pb geochronology of the granitoids of the Dabakala area (Côte d'Ivoire): evidence for a 2.3 Ga crustal growth event in the Paleoproterozoic of West Africa. *Precambrian Research* **127**, 329–54.

Girty MS, Thomson C, Girty GH, Bracchi KA and Miller J (1994) U-Pb zircon geochronology, CLMSZ (Cuyamacañ Laguna Mountains shear zone),

Peninsular Ranges, southern California. *Geological Society of America Abstracts with Programs* **26**, 54.

Giustina MESD, de Oliveira CG, Pimentel MM, de Melo LV, Fuck RA, Dantas EL and Buhn B (2009) U-Pb and Sm-Nd constraints on the nature of the Campinorte sequence and related Palaeoproterozoic juvenile orthogneisses, Tocantins Province, central Brazil. In *Palaeoproterozoic Supercontinents and Global Evolution* (eds SM Reddy, R Mazumder, DAD Evans and AS Collins), pp. 255–69. *Geological Society of London, Special Publication no.* **323**.

Grenholm M, Jessell M and Thebaud N (2019) A geodynamic model for the Paleoproterozoic (2.27-1.96 Ga) Birimian Orogen of the southern West African Craton – insights into an evolving accretionary-collisional orogenic system. *Earth Science Reviews* **192**, 138–93.

Hassen IS, Rasmy El-Gharbawy I, El-Masry NN and Buda G (2008) Geochemistry of the magmatic microgranular enclaves of Wadi Rahaba area, southern Sinai, Egypt. *Acta Mineralogica-Petrographica* **48**, 1–15.

Hastie AR, Kerr AC, Pearce JA and Mitchell SF (2007) Classification of altered volcanic island arc rocks using immobile trace elements: development of the Th-Co discrimination diagram. *Journal of Petrology* **48**, 2341–57.

Heaman LM (1997) Global mafic magmatism at 2.45 Ga: remnants of an ancient large igneous province? *Geology* **25**, 299–302.

Hirdes W and Davis DW (2002) U-Pb geochronology of paleoproterozoic rocks in the southern part of the Kedougou-Kenieba Inlier, Senegal, West Africa: evidence of diachronous accretionnary development of the eburnean province. *Precambrian Research* **118**, 83–99.

Hirdes W, Davis DW and Eisenlohr BN (1992) Reassessment of Proterozoic granitoid ages in Ghana on the basis of U/Pb zircon and monazite dating. *Precambrian Research* **56**, 89–96.

Hirdes W, Davis DW, Ludtke G and Konan G (1996) Two generations of Birimian (Paleoproterozoic) volcanic belts in northeastern Cote d'Ivoire (West Africa), as demonstrated by precise U–Pb mineral dating: consequences for 'Birimian controversy'. *Precambrian Research* **80**, 173–99.

Irvine TN and Baragar WR (1971) A guide to the chemical classification of the common igneous rocks. *Canadian Journal of Earth Science* **8**, 523–48.

Isley AE and Abbott DH (1999) Plume-related mafic volcanism and the deposition of banded iron formation. *Journal of Geophysical Research Solid Earth* **104**, 15461–77.

Jessell MW, Amponsah PO, Baratoux L, Asiedu, DK, Loh GK and Ganne J (2012) Crustal-scale transcurrent shearing in the Paleoproterozoic Sefwi-Sunyani-Comoé region, West Africa. *Precambrian Research* **212–213**, 155–68.

Kesse GO (1985) *The Mineral and Rock Resources of Ghana*, Rotterdam: AA Balkema, 610 p.

Kouamelan AN, Peucat JJ and Delor C (1997) Reliques archéennes (3.15 Ga) au sein du magmatisme Birimien (2.1 Ga) de Côte d'Ivoire, Craton Ouest-African. *Comptes Rendus de l'Académie des Sciences série IIa* **324**, 719–27.

Leube A, Hirdes W, Mauer R and Kesse G (1990) The early Proterozoic Birimian supergroup of Ghana and some aspects of its associated gold mineralization. *Precambrian Research* **46**, 139–65.

Liew TC and Hofmann AW (1988) Precambrian crustal components, plutonic associations, plate environment of the Hercynian Fold Belt of Central Europe: indications from a Nd and Sr isotopic study. *Contributions to Mineralogy and Petrology* **98**, 129–38.

Lompo M (2009) Geodynamic evolution of the 2.25–2.0 Ga Palaeoproterozoic magmatic rocks in the Man-Leo Shield of the West African Craton: a model of subsidence of an oceanic plateau. In *Palaeoproterozoic Supercontinents and Global Evolution* (eds SM Reddy, R Mazumder, DAD Evans and AS Collins), pp. 231–54. Geological Society of London, Special Publication no. 323.

Losiak A, Schulz T, Buchwaldt R and Koeberl C (2013) Petrology, major and trace element geochemistry, geochronology, and isotopic composition of granitic intrusions from the vicinity of the Bosumtwi impact crater, Ghana. *Lithos* **177**, 297–313.

Meert JG (2012) What's in a name? The Columbia (Paleopangaea/Nuna) supercontinent. *Gondwana Research* **21**, 987–93.

Nesbitt HW and Young GM (1982) Early Proterozoic climates and plate motions inferred from major element chemistry of lutites. *Nature* **299**, 715–17.

Othman DB, Polvé M and Allègre CJ (1984) Nd–Sr isotopic composition of granulites and constraints on the evolution of the lower continental crust. *Nature* **307**, 510–5.

Parra-Avila LA, Baratoux L, Eglinger A, Fiorentini ML and Block S (2019) The Eburnean magmatic evolution across the Baoule-Mossi domain: geodynamic implications for the West African Craton. *Precambrian Research.* **332**, 105392.

Parra-Avila LA, Belousova E, Fiorentini ML, Baratoux L, Davis J, Miller J and McCuaig TC (2016) Crustal evolution of the Paleoproterozoic Birimian terranes of the Baoulé-Mossi domain, southern West African Craton: U–Pb and Hf-isotope studies of detrital zircons. *Precambrian Research* **274**, 25–60.

Parra-Avila LA, Belousova E, Fiorentini ML, Eglinger A, Block S and Miller J (2018) Zircon Hf and O-isotope constraints on the evolution of the Paleoproterozoic Baoulé-Mossi domain of the southern West African Craton. *Precambrian Research* **306**, 174–88.

Parra-Avila LA, Kemp AIS, Fiorentini ML, Belousova E, Baratoux L, Block S, Jessell M, Bruguier O, Begg GC, Miller J, Davis J and McCuaig TC (2017) The geochronological evolution of the Paleoproterozoic Baoulé-Mossi domain of the Southern West African Craton. *Precambrian Research* **300**, 1–27.

Pawlig S, Gueye M, Klischies R, Schwarz S, Wemmer K and Siegesmund S (2006) Geochemical and Sr–Nd isotopic data on the Birimian of the Kedougou-Kenieba Inlier (Eastern Senegal): implications on the Palaeoproterozoic evolution of the West African Craton. *South African Journal of Geology* **109**, 411–27.

Pearce JA (1983) Role of the sub-continental lithosphere in magma genesis at active continental margins. In *Continental Basalts and Mantle Xenoliths* (eds CJ Hawkesworth and MJ Norry), pp. 230–249 Cheshire, UK: Shiva Publishing Limited.

Pearce JA (2008) Geochemical fingerprinting of oceanic basalts with applications to ophiolite classification and the search for Archean oceanic crust. *Lithos* **100**, 14–48.

Pearce JA (2014) Immobile element fingerprinting of ophiolites. *Elements* **10**, 101–8.

Pearce JA, Bender JF, De Long SE, Kidd WSF, Low PJ, Güner Y, Saroglu F, Yilmaz Y, Moorbath S and Mitchell JG (1990) Genesis of collision volcanism in eastern Anatolia, Turkey. *Journal of Volcanology and Geothermal Research* **44**, 189–229.

Pearce JA and Peate DW (1995) Tectonic implications of the composition of volcanic arc magmas. *Annual Review of Earth Planetary Science* **23**, 251–85.

Peccerillo A and Taylor SR (1976) Geochemistry of Eocene calc-alkaline volcanic rocks from the Kastamonu area, northern Turkey. *Contributions to Mineralogy and Petrology* **58**, 63–81.

Petersson A, Scherstén A and Gerdes A (2018) Extensive reworking of Archaean crust within the Birimian terrane in Ghana as revealed by combined zircon U-Pb and Lu-Hf isotopes. *Geoscience Frontiers* **9**, 173–89.

Petersson A, Scherstén A, Kemp AIS, Kristinsdóttir B, Kalvig P and Anum S (2016) Zircon U-Pb-Hf evidence for subduction related crustal growth and reworking of Archaean crust within the Palaeoproterozoic Birimian terrane, West African Craton, SE Ghana. *Precambrian Research* **275**, 286–309.

Rajaieh M, Khalili M and Richards I (2010) The significance of mafic microgranular enclaves in the petrogenesis of the Dehno Complex, Sanandaj-Sirjan belt, Iran. *Journal of Asian Earth Sciences* **39**, 24–36.

Roddaz M, Debat P and Nikiéma S (2007) Geochemistry of Upper Birimian sediments (major and trace elements and Nd–Sr isotopes) and implications for weathering and tectonic setting of the Late Paleoproterozoic crust. *Precambrian Research* **159**, 197–211.

Rogers JJW and Santosh M (2002) Configuration of Columbia, a Mesoproterozoic supercontinent. *Gondwana Research* **5**, 5–22.

Rogers JJW and Santosh M (2009) Tectonics and surface effects of the supercontinent Columbia. *Gondwana Research* **15**, 373–80.

Sakyi PA, Anum S, Su BX, Nude PM, Asiedu DK, Nyame FK, Kwayisi D and Su BC (2018a) Geochemical and Sr-Nd isotopic records of Paleoproterozoic metavolcanics and mafic intrusive rocks from the West African Craton: evidence for petrogenesis and tectonic setting. *Geological Journal* **53**, 725–41.

Sakyi PA, Su BX, Anum S, Kwayisi D, Dampare SB, Anani CY and Nude PM (2014) New zircon U–Pb ages for erratic emplacement of 2213–2130 Ma

Paleoproterozoic calc-alkaline I-type granitoid rocks in the Lawra Volcanic Belt of Northwestern Ghana, West Africa. *Precambrian Research* **254**, 149–68.

Sakyi PA, Su BX, Kwayisi D, Chen C, Bai Y and Alemayehu M (2018b) Zircon trace element geochemical constraints on the evolution of the Paleoproterozoic Birimian granitoids of the West African Craton (Ghana). *Journal of Earth Science* **29**, 43–56.

Saunders AD, Norry MJ and Tarney J (1988) Origin of MORB and chemically depleted mantle reservoirs: trace element constrains. *Journal of Petrology* Special Volume, 415–45.

Senyah GA, Dampare SB and Asiedu DK (2016) Geochemistry and tectonic setting of the Paleoproterozoic metavolcanic rocks from the Chirano Gold District, Sefwi belt, Ghana. *Journal of African Earth Science* **122**, 32–46.

Shervais JW (1982) Ti–V plots and the petrogenesis of modern and ophiolitic lavas. *Earth and Planetary Science Letters* **59**, 101–18.

Spencer CJ, Roberts NMW and Santosh M (2017) Growth, destruction, and preservation of Earth's continental crust. *Earth-Science Reviews* **172**, 87–106.

Srivastava RK, Ellam RM and Gautam GC (2009) Sr-Nd isotope geochemistry of the early Precambrian sub-alkaline mafic igneous rocks from the southern Bastar craton, Central India. *Mineralogy and Petrology* **96**, 71–79.

Sun SS and McDonough WF (1989) Chemical and isotopic systematics of oceanic basalts: implication for mantle composition and processes. In *Magmatism in the Ocean Basins* (eds AD Saunders and MJ Norry), pp. 313–45. *Geological Society of London, Special Publication no.* **42**.

Sylvester PJ and Attoh K (1992) Lithostratigraphy and composition of 2.1 Ga greenstone belts of the West African Craton and their bearing on crustal evolution and the Archean-Proterozoic boundary. *Journal of Geology* **100**, 377–93.

Taylor PN, Moorbath S, Leube A and Hirdes W (1992) Early Proterozoic crustal evolution in the Birimian of Ghana: constraints from geochronology and isotope geochemistry. *Precambrian Research* **56**, 97–111.

Thiéblemont D, Delor C, Cocherie A, Lafon JM, Goujou J-C, Baldé A, Bah M, Sané H and Mark Fanning CM (2001) A 3.5 Ga granite–gneiss basement in Guinea: further evidence for early Archean accretion within the West African Craton. *Precambrian Research* **108**, 179–94.

Wood DA (1980) The application of a Th-Hf-Ta diagram to problems of tectonomagmatic classification and to establishing the nature of crustal contamination of basaltic lavas of the British Tertiary volcanic province. *Earth and Planetary Science Letters* **50**, 11–30.

Wu F, Zhao G, Simon A, Wilde SA and Sun D (2005) Nd isotopic constraints on crustal formation in the North China Craton. *Journal of Asian Earth Sciences* **24**, 523–45.

Yücel C, Arslan M, Temizel I, Abdioğlu E and Ruffet G (2017) Evolution of K-rich magmas derived from a net veined lithospheric mantle in an ongoing extensional setting: geochronology and geochemistry of Eocene and Miocene volcanic rocks from Eastern Pontides (Turkey). *Gondwana Research* **45**, 65–86.

Zhang HF, Sun M, Lu FX, Zhou XH, Zhou MF, Liu YS and Zhang GH (2001) Geochemical significance of a garnet lherzolite from the Dahongshan kimberlite, Yangtze Craton, southern China. *Geochemical Journal* **35**, 315–31.

Zhao G, Cawood PA, Wilde SA and Sun M (2002) Review of global 2.1–1.8 Ga collisional orogens and accreted cratons: a pre-Rodinia supercontinent? *Earth Science Reviews* **59**, 125–62.

Zhao G, Sun M, Wilde SA and Li S (2004) A Paleo-Mesoproterozoic supercontinent: assembly, growth, and breakup. *Earth Science Reviews* **67**, 91–123.

Zhou MF, Kennedy AK, Sun M, Malpas J and Lesher CM (2002) Neo-Proterozoic arc-related mafic intrusions in the northern margin of South China: implications for accretion of Rodinia. *Journal of Geology* **110**, 611–8.